REPORT DOCUMENTATION PAGE

1. REPORT DATE (DD-MM-YYYY) 21-03-2012	2. REPORT TYPE Thesis	3. DATES COVERED (From - To)

4. TITLE AND SUBTITLE EMIIM Wetting Properties & Their Effect on Electrospray Thruster Design	5a. CONTRACT NUMBER
	5b. GRANT NUMBER
	5c. PROGRAM ELEMENT NUMBER
6. AUTHOR(S) Garrett D. Reed	5d. PROJECT NUMBER
	5f. WORK UNIT NUMBER 33SP0706

7. PERFORMING ORGANIZATION NAME(S) AND ADDRESS(ES) Air Force Research Laboratory (AFMC) AFRL/RZSS 1 Ara Drive Edwards AFB CA 93524-7013	8. PERFORMING ORGANIZATION REPORT NUMBER

9. SPONSORING / MONITORING AGENCY NAME(S) AND ADDRESS(ES) Air Force Research Laboratory (AFMC) AFRL/RZS 5 Pollux Drive Edwards AFB CA 93524-7048	10. SPONSOR/MONITOR'S ACRONYM(S)
	11. SPONSOR/MONITOR'S NUMBER(S) AFRL-RZ-ED-TP-2012-082

12. DISTRIBUTION / AVAILABILITY STATEMENT

Approved for public release; distribution unlimited (PA #12227).

13. SUPPLEMENTARY NOTES
A thesis submitted to California State University, Northridge, CA, in partial fulfillment of the requirements for the degree of Master of Science in Mechanical Engineering

14. ABSTRACT

Recent advances in the development of highly conductive ionic liquids have made them of interest for use as propellant in spacecraft propulsion systems. Electrospray thrusters apply strong electrostatic fields to an ionic liquid in order to extract and accelerate charged particles/droplets, producing thrust. The behavior of these ionic liquids as they pass through the components of an electrospray system can have a significant effect on thruster operation. The wetting and adhesion behavior between the ionic liquid propellant and solid materials can be characterized using the surface tension and contact or "wetting" angle formed when a liquid droplet comes in contact with a solid surface. Ideally this angle is a function of the interactions between the solids surface energy, the surface tension of the liquid and the interactions of both with the surrounding medium. Deviation from ideal contact angle behavior can indicate surface inconsistencies, environmental effects or contamination of the solid and liquid. Contact angle and surface tension measurements are presented for the ionic liquid propellant 1-Ethyl-3-methylimidazolium bis(triuoromethylsulfonyl)imide, called EMIIm or EtMeImTf$_2$N, with respect to various substrate materials and environmental conditions. Analysis of these measurements determines optimum materials and operating conditions for current and future electrospray thruster designs.

15. SUBJECT TERMS

16. SECURITY CLASSIFICATION OF:			17. LIMITATION OF ABSTRACT	18. NUMBER OF PAGES	19a. NAME OF RESPONSIBLE PERSON Dr. William R. Hargus, Jr.
a. REPORT Unclassified	b. ABSTRACT Unclassified	c. THIS PAGE Unclassified	SAR	75	19b. TELEPHONE NUMBER (include area code) N/A

CALIFORNIA STATE UNIVERSITY, NORTHRIDGE

EMIIM WETTING PROPERTIES & THEIR EFFECT ON ELECTROSPRAY
THRUSTER DESIGN

A thesis submitted in partial fulfillment of the requirements
For the degree of Master of Science in Mechanical Engineering

By

Garrett Donald Reed

March 2012

The thesis of Garrett Donald Reed is approved:

_____	_____
Dr. Timothy W. Fox	Date
_____	_____
Dr. Michael R. Holmes	Date
_____	_____
Dr. Sidney H. Schwartz	Date

California State University, Northridge

This thesis is dedicated to my wife Nicole and mother Rhonda. They are the two strongest people I have ever known, and it is no coincidence that they are also the women I love.

Table of Contents

Theory 13

Appendix **54**

List of Figures

List of Tables

Abstract

EMIIM WETTING PROPERTIES & THEIR EFFECT ON ELECTROSPRAY
THRUSTER DESIGN

By

Garrett Donald Reed

Master of Science in Mechanical Engineering

Recent advances in the development of highly conductive ionic liquids have made them of interest for use as propellant in spacecraft propulsion systems. Electrospray thrusters apply strong electrostatic fields to an ionic liquid in order to extract and accelerate charged particles, producing thrust. The behavior of these ionic liquids as they pass through the components of an electrospray system can have a significant effect on thruster operation. The wetting and adhesion behavior between the ionic liquid propellant and solid materials can be characterized using the surface tension and contact or "wetting" angle. Ideally this angle is a function of the interactions between the solids surface energy, the "free" surface energy or tension of the liquid and the interactions of both with the surrounding medium. Deviation from ideal contact angle behavior can indicate surface inconsistencies, environmental effects or contamination of the solid or liquid. Contact angle and surface tension measurements are presented for the ionic liquid propellant 1-Ethyl-3-methylimidazolium bis(trifluoromethylsulfonyl)imide, called EMIIm or $EtMeImTf_2N$, with respect to various substrate materials and environmental conditions. Analysis of these measurements determines optimum materials and operating conditions for current and future electrospray thruster designs.

Nomenclature

A	Surface area	m^2
A_θ	Surface area of sessile droplet base	m^2
AFRL	Air Force Research Laboratory	
b	Radius of an un-chamfered emitter tip	m
B	Empirical constant for calculating contact angles	-
CAS	Chemical Abstracts Service	
$D_{\theta C}$	Critical droplet diameter	m
DRS	Disturbance Reduction System	
EMIIm	1-Ethyl-3-methylimidazolium bis(trifluoromethylsulfonyl)imide	
EP	Electric propulsion	
ESA	European Space Agency	
FTA	First Ten Angstroms	
g	Acceleration due to gravity	$9.8 \frac{m}{s^2}$
G	Gibbs excess free energy	J
H	Contact angle hysteresis	$\circ$
JPL	Jet Propulsion Laboratory	
k	Empirical constant describing dynamic contact angle behavior	-
K	Constant used in Eotvos Rule	$JK^{-1} \left(mol^{\frac{2}{3}} \right)$
L_c	Capillary length	m
LISA	Laser Interferometer Space Antenna	
I_{sp}	Mass Specific Impulse	s
MN	Model Number	
n	Empirical constant describing dynamic contact angle behavior	-
N_j	Number of excess moles of the jth component	—
NASA	National Aeronautics and Space Administration	
P	Pressure	$\frac{N}{m^2}$
P_0	Vapor pressure of a liquid	$\frac{N}{m^2}$
PC	Personal Computer	
PN	Part Number	
PTFE	Polytetrafluoroethylene, teflon substrate	
ppm	Parts per million	-
r_i	Radius of curvature	-
r_θ	Radius of the sessile droplet base	m
r_s	Ratio of actual surface area to apparent surface area due to roughness	-
R_a	Averaged surface roughness	m

R	The gas constant	m
Si	Undoped silicon substrate, high polish	
SMART	Small Mission for Advanced Research in Technolgy	
STIL	Sciences et Techniques Industrelles de la Lumière	
SS316C	316 stainless steel substrate with coarse grit sandblasted surface	
SS316F	316 stainless steel substrate with fine grit sandblasted surface	
SS316M	Mirror finish 316 stainless steel substrate	
t	Time elapsed from liquid/solid initial contact	s
T	Absolute temperature	K
T_C	Critical temperature of the test liquid	K
Ti	Titanium substrate	
V	Molar volume of the test liquid	$\frac{m^3}{mol}$
W	Tungsten substrate, un-sintered	
W_r	Reversible, isentropic work	J
β	The modified bond number	-
ΔP	Upstream pressure acting on electrospray propellant	$\frac{m}{s}$
ΔV	Change in velocity due to forces acting upon a spacecraft	$\frac{m}{s}$
ϕ	Emitter tip chamfer angle	$^\circ$
γ	Surface free energy	$\left(\frac{N}{m}\right)$
γ_{lv}	Surface free energy of the test liquid, synonymous with surface tension	$\left(\frac{J}{m^2}\right)$
γ_{sv}	Surface energy of a solid surface in presence of a vapor	$\left(\frac{J}{m^2}\right)$
γ_{s0}	Surface energy of a solid surface in vacuum	$\left(\frac{J}{m^2}\right)$
γ_{sl}	Interfacial energy between liquid and solid contact area	$\left(\frac{J}{m^2}\right)$
Γ_{sv}	Gibb's surface excess of vapor on a solid surface	J
μ	The dipole moment	$(C \times m)$
π_{sv}	Spreading pressure	$\left(\frac{J}{m^2}\right)$
π_{lv}	Adhesion tension or energy	$\left(\frac{J}{m^2}\right)$
θ	Idealized contact angle	$^\circ$
θ'	Measured contact angle	$^\circ$
θ_A	Advancing contact angle as sessile droplet volume increases	$^\circ$
θ_R	Receding contact angle as sessile droplet volume decreases	$^\circ$
θ_W	Effective contact angle due to surface roughness effects	$^\circ$
θ_Z	Contact angle calculated using Eötvös Rule	$^\circ$
ρ_l	Density of the test liquid	$\frac{kg}{m^3}$
ρ_v	Density of the surrounding vapor	$\frac{kg}{m^3}$

Introduction

Spacecraft & Electric Propulsion

In its broadest sense spacecraft propulsion includes any mechanism used to affect the motion of a spacecraft. The term encompasses a wide variety of mechanisms which, depending upon mission goals, may serve to prevent orbit decay, aim the spacecraft, perform orbit transfer maneuvers or provide the acceleration necessary for traveling intra-stellar distances. Thrusters are devices used to convert stored potential energy into useful kinetic energy by means of expelling a propellant. The resulting force, described by Newton's third law of motion, changes the velocity and position of the spacecraft.

Thrusters can generally be segregated into chemical, electric and hybrid propulsion systems. Chemical propulsion thrusters rely on a pressure differential, generated by an exothermic reaction, to produce thrust. These thrusters rely on the innate energy contained in the propellants chemical bonds, which may consist of a single component such as hydrazine in the presence of a catalyst (a mono propellant) or a two component fuel-oxidizer (bi propellant) reaction. Though capable of higher thrust ($\sim 10^6$ Newtons), chemical propulsion is "propellant limited"; the total ΔV produced by a chemical system is limited by the mass and energy density of the propellant stored.[1][2]

Electric propulsion (EP) utilizes electrostatic, electrothermal or electromagnetic forces acting on a propellant to produce thrust. EP thrusters typically increase the energy level of a propellant through ionization, ablation or resistive heating and then accelerate the energized propellant using electric/magnetic fields. A significant advantage of EP thrusters is that they are "power limited"; the amount of ΔV available is primarily limited by the amount of electrical power that can be gathered and stored by the spacecraft. As a result EP thrusters are typically less massive, and offer much higher propellant utilization efficiency (~ 1000's of seconds I_{sp}), when compared to chemically powered systems.[1][2] This means that, per unit mass of fuel, EP can provide much more ΔV than chemical propulsion, reducing the propulsion system mass needed to complete a given mission goal. This benefit comes at a cost though, as EP thrusters operate at much lower thrust levels compared to chemical propulsion. To compensate for this an EP thruster might fire continuously for much longer durations than a chemical thruster in order to affect the same ΔV. EP thrusters are ideally suited for missions were reduced propulsion system mass, longer spacecraft lifetime and greater mission ΔV are required.

Electrosprays

Electrospray thrusters are an electrostatic form of EP that uses an ionic liquid propellant and electric field(s) to produce thrust. Electrosprays consist of a liquid emitter and electrode
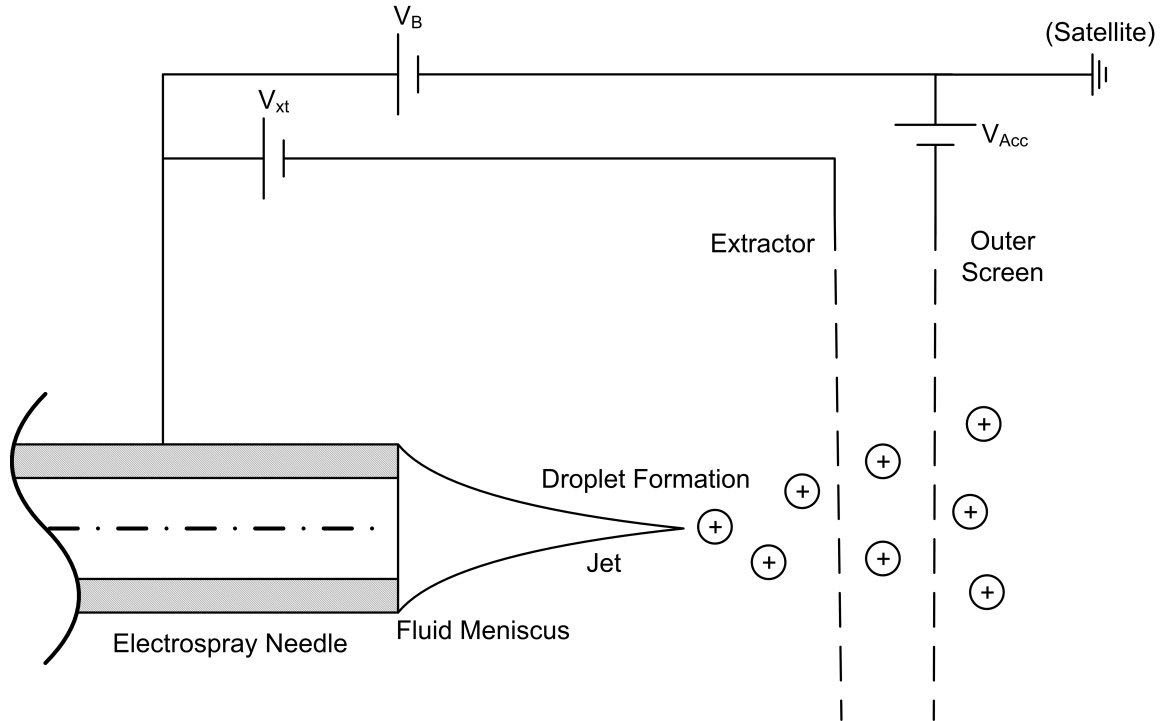
Figure 1: Functional Diagram of an electrospray thruster.

grid(s) used for extracting and accelerating particles or droplets from the ionic liquid. Emitters can be internally or externally wetted "needles" of small diameter (~$100\mu m$ diameter), porous cones, or simply a uniform opening through which propellant can flow.[3][4][5][6] A picture of different emitter types is shown in Figure 2. Ionic liquid propellant flows to the emitter opening under forced pressure or capillary action and is charged to a high voltage potential. An opposing potential is applied to the closest "extraction" grid. The opposing charges in close proximity to each other cause a Lorentz force to act upon the charged liquid. Due to the interaction between the Lorentz force and the propellants' surface tension, the liquid forms a "Taylor cone" at the tip of emitter.[5] The tip of this cone consists of particles charged opposite to the extractor grid and of like charge to the emitter. A Taylor cone formed using an internally wetted emitter and the ionic liquid BMI-BG$_4$ is shown in Figure 3.[7] Emitters are precisely aligned with openings present in the electrode grid that allow the ionized droplets or particles to pass through the grid without obstruction. Depending on the operating polarity and characteristics of the ionic liquid propellant, small ionized particles or fine droplets ($10nm - 10\mu m$ diameter) of the liquid detach from the Taylor cone and accelerate through the extraction grid.[8][9] A second "acceleration" grid, charged to an even greater voltage potential, can be used to further accelerate the droplet in order to achieve higher I_{sp}. Under continuous operation this provides a steady spray of mass accelerating away, producing thrust. A functional diagram of a typical electrospray system is shown in Figure 1.

Electrospray thrusters were first investigated in the 1960's, though largely abating during the 1980's and 90's.[4][6] Due to recent advances in micro electromechanical systems (MEMS) fabrication, the development of ionic liquids, and interest in small scale propul-

2
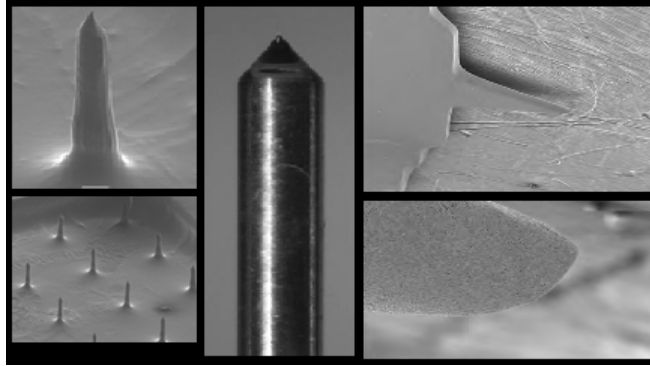
Figure 2: Emitters from left to right: externally wetted array with close-up, internally wetted, porous tip with close-up.
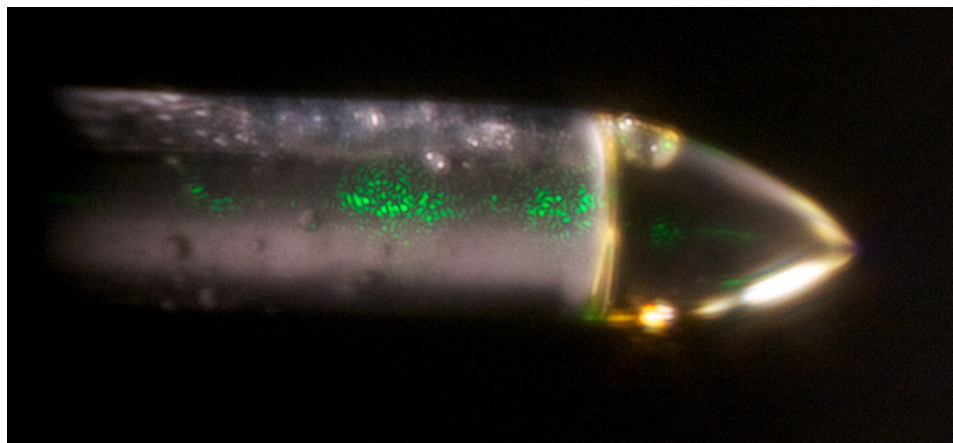
Figure 3: Picture of a Taylor cone formed at AFRL, note bubbles present.

sion, there has been a resurgence in electrospray research and development. Electrosprays offer a low noise to thrust ratio and show promise for scaling within a large range of desired system mass and I_{sp} (100-1000's of seconds).[3][5] Scaling is accomplished by creating arrays of emitters and grid openings. An example of a single versus arrayed grid is shown in Figure 4. Depending on design, electrosprays are also capable of operating under alternating polarity. This conveniently avoids an undesirable net charge build up on the spacecraft that would otherwise require an anode/cathode to neutralize. Electrosprays also show potential for using propellants that are compatible with some chemically powered propulsion systems, providing multiple thrust options using a common fuel reservoir and feed system. Thanks in part to recent advances in the development of alternatives to organic solvents, a variety of ionic liquids are now available for use as electrospray propellant, though many of their properties and interactions remain un-investigated.[10]
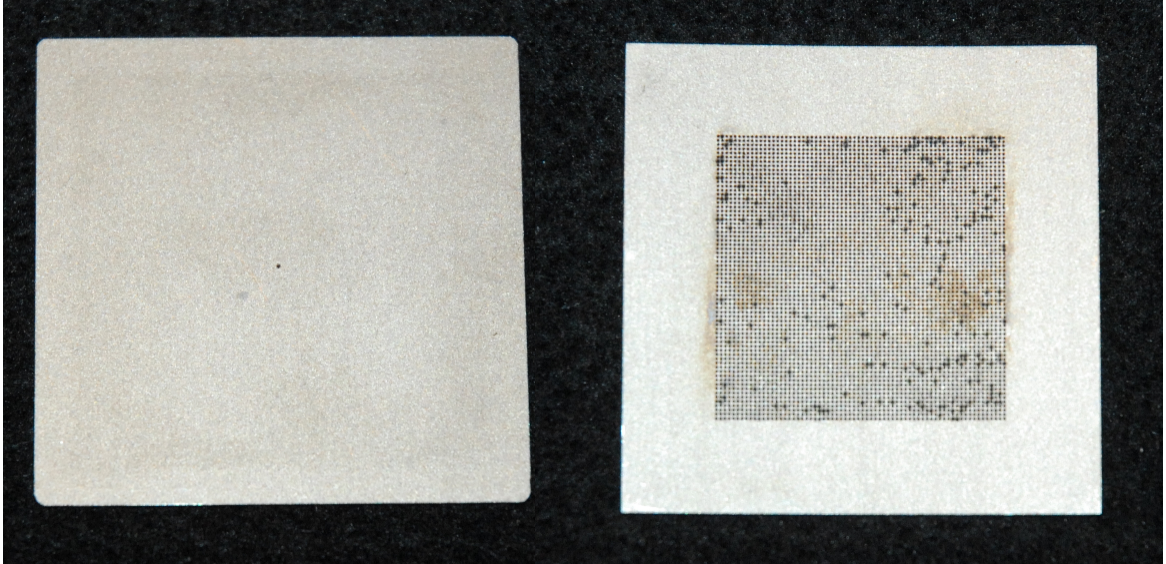
Figure 4: Titanium electrode grids in use at AFRL, single (L), 70x70 array (R).

Contemporary Research & Literature Review

The significance of propellant wetting behavior with respect to electrospray operation have been described by multiple researchers.[3][5][6][11][12] It has been shown that material wetting affects Taylor cone formation, propellant feed systems and overall reliability of electrosprays. Several methods have been developed to either inhibit or promote wetting between ionic liquid propellants and various solid electrospray components. These include the choice of component materials, thin film surface coatings that have a desired high or low wettability, changing the solid component surface roughness and varying operating temperature.[4][13][14]

An electrospray thruster has been developed by NASA JPL, and is scheduled to launch in April of 2012 on the LISA Pathfinder spacecraft as part of the DRS payload.[9][15] Lisa Pathfinder is part of the ESA's SMART program. This will be the first on-flight demonstration of an electrospray thruster system. Two electrospray clusters will be used as a technology demonstration, providing propulsion to counteract drag effects on the spacecraft.[9] The design uses an internally wetted emitter and the ionic liquid propellant 1-Ethyl-3-methylimidazolium bis(trifluoromethylsulfonyl)imide, called EMIIm.[3] During research and development of this system it was concluded by Conroy et. al. and others that the wetting characteristics of EMIIm in contact with solid emitter materials can have an effect on thruster performance and reliability.[3] It was concluded during this research that wetting behavior can affect bubble formation in the propellant feed system.[3] As these bubbles pass through the feed system they introduce compressibility, causing excessive propellant accumulation at the emitter tip and inconsistency in thruster fire timing. If the excess propellant on the emitter tip grows large enough it can allow arcing between the emitter and the extractor grid, shorting the circuit.[3][4][16] Additionally if errant propellant droplets strike the extractor or acceleration grids, an accumulation can form that may block the spray

4

aperture. Conroy et. al. specifically cite the need for additional data on wetting angles for EMIIm in combination with different materials suitable for electrospray use.

Motivation for This Research

Due to their recent development many of the properties of specific ionic liquids such as EMIIm and their interactions with different solid materials are unknown. The liquid surface tension of EMIIm is well characterized however its wetting behavior in contact with different solid materials is not. The following research presents measurements and analysis of EMIIm wetting properties when in contact with different solids, varying surface roughnesses, and under different operating conditions. Wetting properties are characterized using contact angle measurements taken using goniometer-sessile drop technique. We also examine the surface tension of the liquid for comparison using the pendant drop method. Measurements are taken with EMIIm and different solid substrates typically used to form electrospray emitters and extraction/acceleration grids. This research will provide insight as to the ideal conditions and suitable materials for optimal electrospray thruster design.

Apparatus

All measurements were taken at and funded by the Unites States Air Force Research Laboratory, Edwards Air Force Base California, spacecraft propulsion directorate. Measurements included contact angles for EMIIm wetting eleven different solid substrates, surface tension and water content for EMIIm. The following describes the experimental apparatus and techniques used to take these measurements and the specific materials tested.

EMIIm

1-Ethyl-3-methylimidazolium bis(trifluoromethylsulfonyl)imide (CAS# 174899-82-2) is a low vapor pressure ionic liquid at room temperature. It has several properties that make it suitable as an electrospray propellant. These properties include relatively low viscosity, high conductivity, negligible vapor pressure and a large charge carrying capacity per unit mass (charge to mass ratio).[3] It is variously referred to as EMIIm, $EtMeImTf_2N$, $[C_2MIM][NTf_2]$ or $[emim] - [Tf_2N]$ by different researchers.[3][10][17][18] For brevity this paper refers to 1-Ethyl-3-methylimidazolium bis(trifluoromethylsulfonyl)imide as EMIIm. The EMIIm obtained for this research was purchased from Strem Chemicals Inc., Newburyport, MA 01950. The EMIIm came in capped, wax sealed bottles packed with dry nitrogen.

It has been reported by several researchers that EMIIm and many ionic liquids are hygroscopic, absorbing ambient atmospheric moisture when exposed.[3][19] At odds with this hygroscopic behavior, Pan et. al. state that EMIIm is also part of a group of, "hydrophobic room-temperature ionic liquids".[17] This behavior was verified during this research. A sample of EMIIm was mixed with water. The water formed a clearly separate layer on top of the EMIIm. This showed that EMIIm is not noticeably miscible with water, making it an extremely weak or non-electrolyte.

Water contamination affects the accuracy of contact angle and surface tension measurements and is described in the analysis section. The water content of the EMIIm obtained for this research is claimed by Strem to be less than 1%. This was verified using Karl-Fisher titration, carried out by the AFRL analytical lab. Results showed that EMIIm, taken from a factory sealed bottle, immediately after opening, had a water content of 2411 ppm $\pm$ 41 ppm by mass. The same test taken on waste EMIIm, that had been exposed to ambient atmosphere for several months, had a water content of 2825ppm $\pm$ 16ppm by mass. This would indicate an approximate %17 increase in water content over the duration of the entire test schedule. These values can be compared with water content values for EMIIm published by Kilaru (1090 ppm), Wandschneider (200 ppm) and Carvalho (42 ppm).[10][18][20]
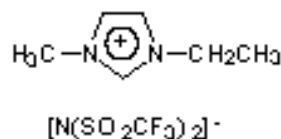
Figure 5: (Left) Molecular Structure of EMIIm. (Right) Sealed 5 gram (3.28 mL) bottle of EMIIm.

Table 1: EMIIm Properties (at 1 ATM, 20 °C)

Property	Value	Units
Formula	$[C_6H_{11}N_2]$+$[N(SO_2CF_3)_2]$	
Density[21]	1523.6	$kg\left(m^{-3}\right)$
Vapor Pressure[3][10]	Negligible	
Surface Tension*	38.1	$J\left(m^{-2}\right)$
Thermal Expansion Coefficient[18]	$6.47e10^{-4}$	K^{-1}
Critical Temperature[10]	1123	K
Molar Volume[17]	$2.58e10^4$	$m^3\left(mol^{-1}\right)$
Kinematic Viscosity[17]	$2.13e10^{-5}$	$\frac{m^2}{s}$

* Measured during this research

Contact Angle & Surface Tension

Measurements were made using a First Ten Angstroms model 125 surface tension and contact angle instrument shown below in Figure 6.[22] The FTA125 consists of an analog NTSC camera for capturing video or still images of the syringe needle tip, droplet and substrate. The camera is oriented vertically while the droplet and substrate are oriented 3° off horizontal, inclined towards turning mirror located below the camera. The slight incline allows full view of the droplet base as it rests on the substrate. The 90° turning mirror allows the camera a side-view of the inclined droplet and substrate. A diagram of this imaging system is shown in Figure 6. This system provides for real time video monitoring and recording as the droplet forms at the syringe tip (a "pendant drop") and after the droplet has been deposited on the substrate surface. The FTA32 ran on a Microsoft Windows$^©$ PC and provided video drop shape analysis allowing both static and time resolved measurements of surface tension and contact angle, droplet volume, diameter and several other geometry-based measurements. An example surface energy tension measurement is shown

in Figure 7. The FTA125 was calibrated using a sapphire lens standard, 6mm in diameter, embedded in an aluminum carrier block forming a 90° angle, also purchased from FTA (PN: L100-001).

Several modifications were made in order to operate the system remotely in a vacuum chamber and allow temperature control and feedback. These modifications allowed multiple test droplets to be dispensed on fresh substrate without re-pressurizing from vacuum. This was accomplished using a remotely actuated, servo motor driven, stage to move the substrate sample back and forth, exposing new substrate material. Multiple droplets could then be dispensed, maximizing the number of measurements possible without re-pressurizing the chamber. A second stepper motor driven plunger allowed remotely controlled dispensing of fluid at a consistent flow rate. The stepper motor, plunger and fluid reservoir were inverted to allow fluid to be dispensed under vacuum without allowing the entire reservoir to continuously drip onto the substrate. This problem was initially observed with the original FTA125 setup. A consequence operating in vacuum is that there is an insufficient pressure differential to keep the fluid suspended in the reservoir, as would normally occur under ambient pressure. A functional diagram of the entire system is pictured in Figure 9.
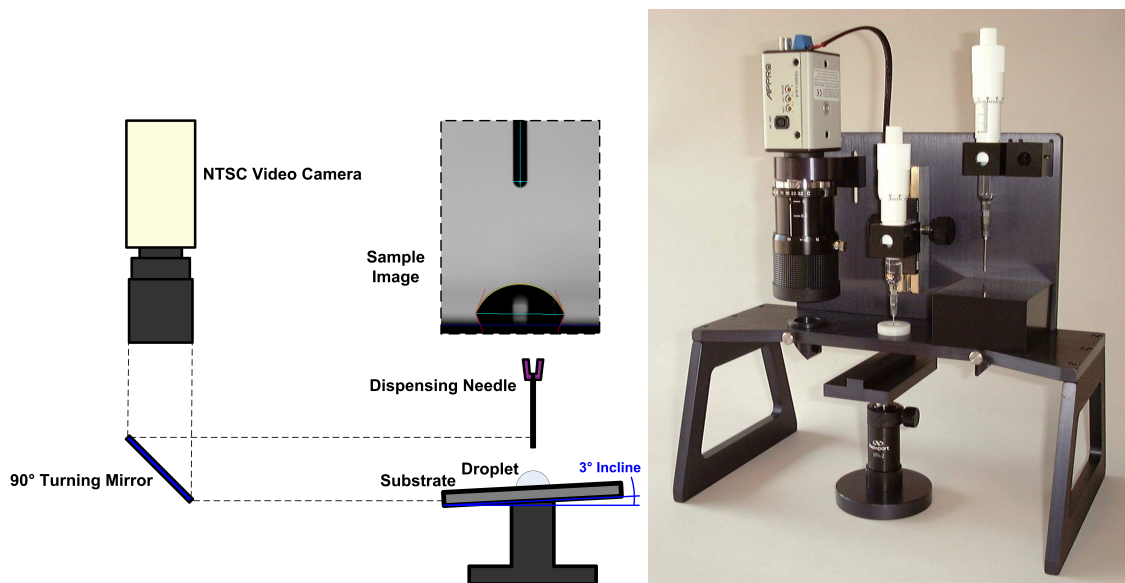
Figure 6: Diagram of FTA125 imaging method (left). Picture of standard FTA125 instrument.

Temperature

Temperature controls were added in order to vary the temperature of the solid substrate, test fluid and ambient air (when testing in atmosphere). Substrates were mounted on a copper plate brazed with copper tubing that could be heated or cooled using a PolyScience
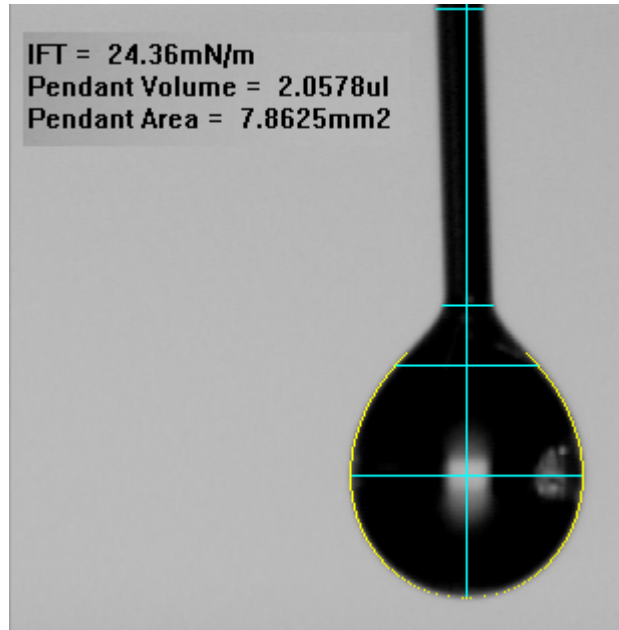
Figure 7: Example of a surface tension measurement taken with the FTA125.

6 Liter reservoir, re-circulating fluid bath system, capable of temperature ranges between -20 and 150° Celsius. The heating and cooling fluid used was ethylene glycol. The bath was also used to heat and cool the custom machined stainless steel reservoir that the fluid passed through before being dispensed. This allowed control of the fluid temperature immediately before coming to the end of the needle tip. The internal air temperature of the vacuum chamber was controlled during atmospheric pressure testing using an incandescent 360 watt projector lamp heating a aluminum radiator. Internal chamber air was circulated over radiator using an 80mm PC fan. The fan was disengaged during actual measurements. With this system it was possible to heat the internal air temperature of the chamber to 70° Celsius, though at this temperature the FTA125 camera electronics began to show signs of overheating.

Temperature measurements were made using five Omega K-type thermocouples (PN: KMQXL-032U-6). Temperatures were measured at the following locations: substrate surface, copper cooling/heating plate interior, stainless steel fluid channel interior, fluid reservoir exterior and in ambient air/vacuum. The location of each of these measurements are illustrated in Figure 9. Thermocouple signals were digitized using a National Instruments Fieldpoint bank (PN's: FP-1601 & FP-TC-120) and recorded to file using LabVIEW 7. These K-type thermocouples are specified as having a 2.8° drift.

Pressure

The FTA125 instrument and temperature controls were installed in vacuum Chamber #8, a bell jar vacuum chamber capable of 10^{-6} Torr pressures, with an interior working volume

of 80 liters. Vacuum was achieved using a two stage system, the first stage being a Varian Triscroll 600 oil-less pump (PN: PTS06001UNIV). First stage pressures achieved were on the order of 10^{-3} torr. The second stage was a Varian TV301 turbopump with a Varian V-301 turbopump controller. Pressure measurements were provided using two MKS pirani gages (PN: 103170010SH) and an MKS Series 943 cold cathode gage digitized by an MKS 937A pressure gage controller.
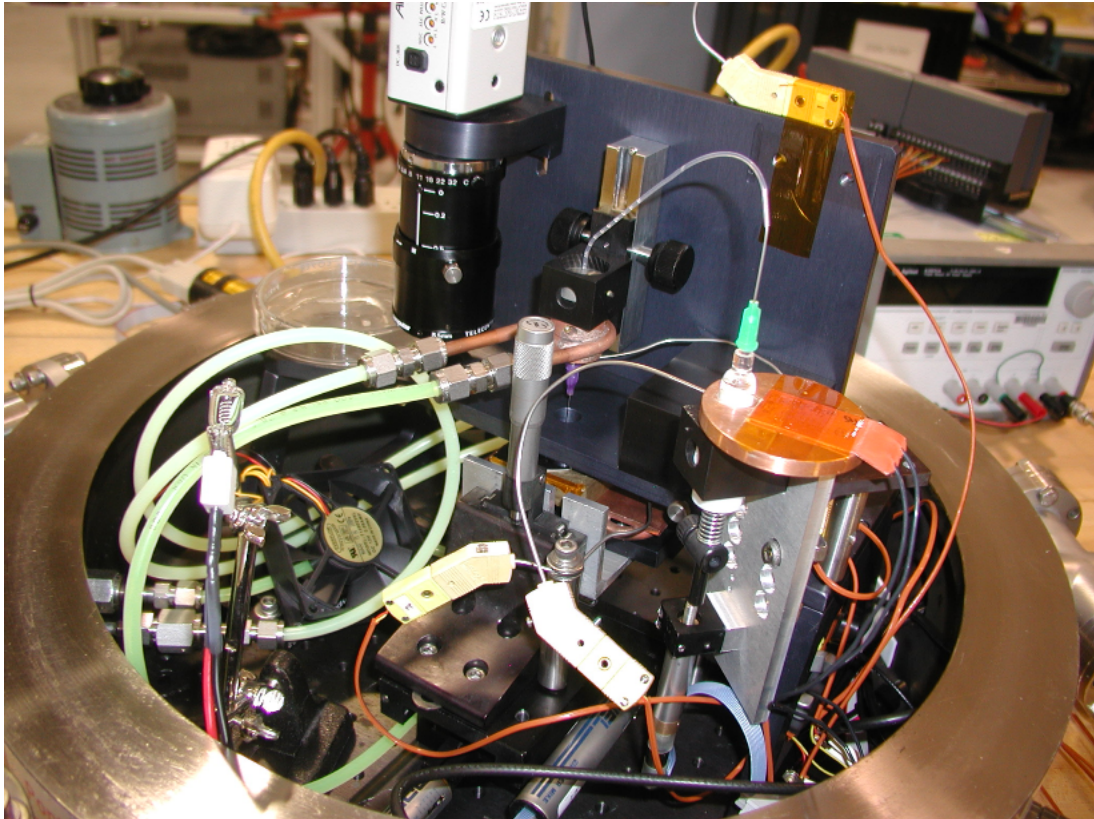
Figure 8: Experimental setup, modified FTA125 installed in vacuum Chamber #8 at AFRL.

Substrates

Substrate materials were selected based on their history of use with electrospray systems and desirable properties for different components. Silicon has been used as an emitter material in multiple electrospray systems.[14][5][23] Similar materials include Pyrex, Kapton (polymide) and fused silica. Extraction and acceleration grids have been made from a variety of metals including tungsten and titanium. Many electrospray components including body and flow fittings are made of stainless steel. PTFE Teflon is also used in propellant feed lines and reservoirs, and has also been proposed as coating for different components. With this in mind, eleven materials were obtained to test with. Three of these substrates

were the same material (stainless steel 316) each with a different surface roughness ranging from mirror polish to sandblasted with coarse grit. Each material, its thickness and measured surface roughness value R_a are listed in Table 2

Table 2: List of Substrates

Material	Thickness[mm]	Roughness (Ra) [μm]	Supplier
Fused Silica	0.5	<0.144	University Wafer
Soda Lime Glass	1	<0.144	Corning Glass Works
Kapton	0.05	0.144	McMasterCarr
PTFE Teflon	1.38	1.47	McMasterCarr
Pyrex	1	<0.144	Esco Products Inc.
Annealed Titanium	13	0.600	McMasterCarr
Unsintered Tungsten	1	0.351	MetalCutting Inc.
Undoped Silicon	0.5	<0.144	University Wafer
Stainless Steel 316 Alloy	4.7	0.634 / 1.20 / 2.52	McMasterCarr

Cleanliness

In order to minimize surface contamination of the substrate, a cleaning regimen was performed before each test. The first step involved placing the substrate in a clean Pyrex petri dish and cleaning the substrate surface with acetone and Kimberly-Clark® Kimwipes EX-L. The substrate was then rinsed with de-mineralized water. Afterwards the petri dish and substrate were heated to approximately 120° Celsius for 20 minutes using a hotplate to vaporize any remaining water. The petri dish was then covered, and allowed to cool to ambient temperature. The substrate would then be installed onto the copper heating/cooling plate minutes before testing. Occasionally small fibers and debris could be seen on the substrate surface image. Visible contaminants were avoided by moving them out of the way using the servomotor stage system described previously. As will be discussed in the analysis section, contamination of the substrate surface or test fluid is one primary sources of inaccuracy associated with contact angle and surface tension measurements.
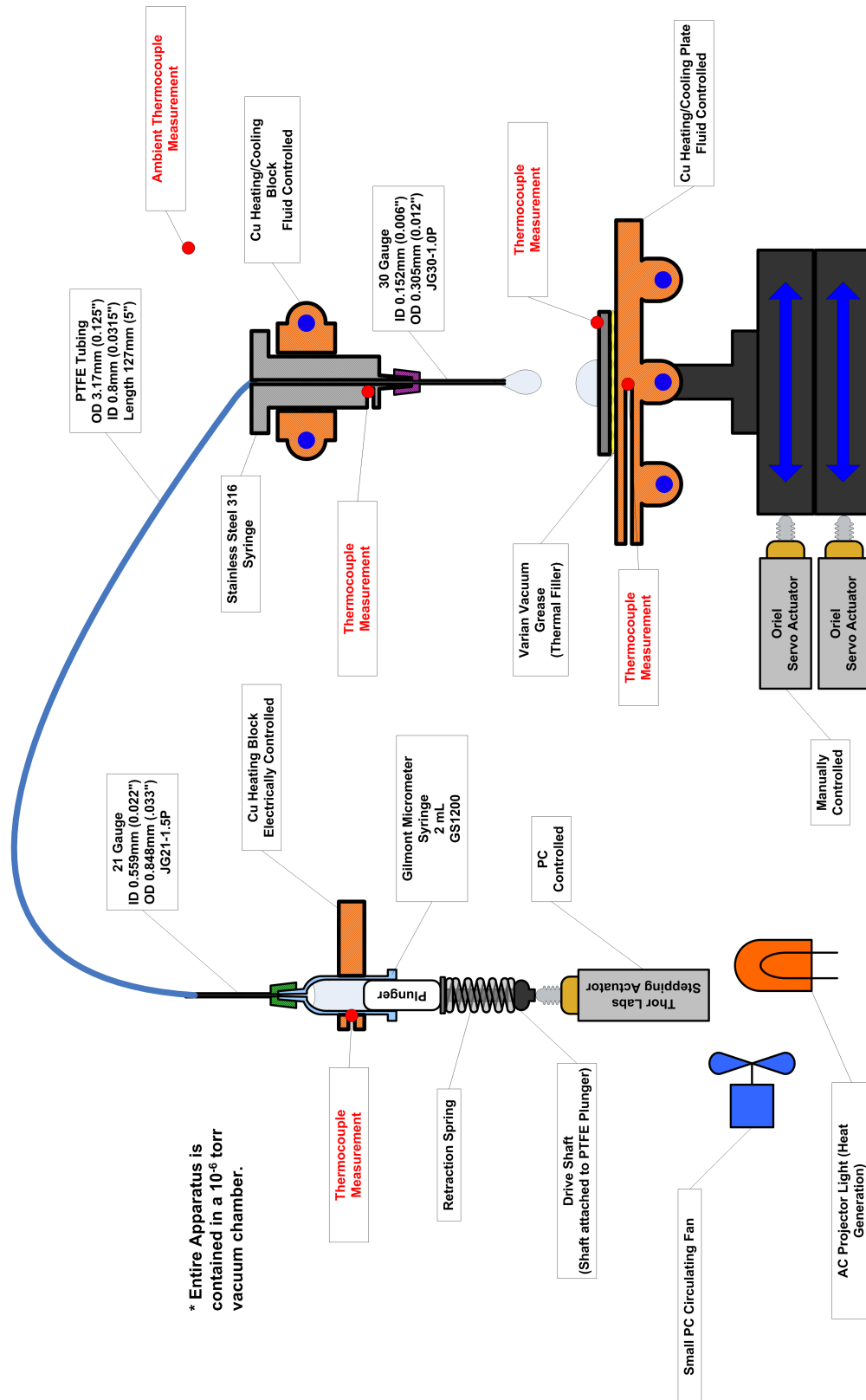
Figure 9: Diagram of the experimental apparatus and its main components.

Theory

Wetting occurs when a liquid comes into contact with, and adheres to a solid, displacing the initial surrounding medium (typically a gas or liquid). The amount of wetting is a function of the intrinsic properties of and interactions between the solid, liquid and surrounding medium. Analysis of these properties and interactions can be extremely complex depending on the many factors that can effect the system before and during wetting. Basic surface energetics theory and observations allow us to understand the amount of wetting that occurs between a given liquid/solid combination and the mechanisms that drive this behavior.

One method of characterizing wetting is by analyzing a single droplet, called a Sessile droplet, resting on a solid surface, surrounded by a gas or liquid medium. This technique allows us to quantify the wetting or "contact" angle θ, formed by the liquid droplet and solid surface plane. An illustration of how this angle is measured can be seen in Figure 10. The contact angle is a useful measure of wettability that reveals information about
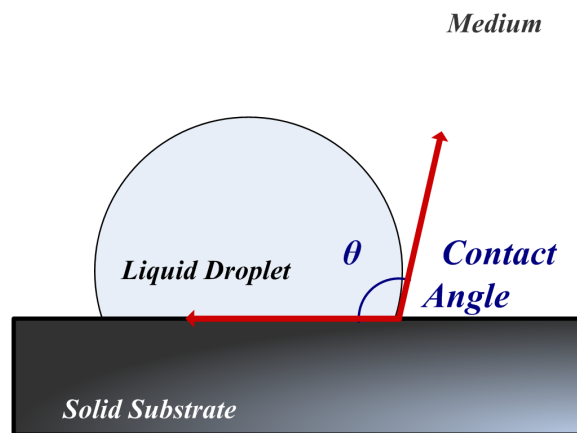
Figure 10: Diagram of a high (greater than 90°) contact angle

the surface energetics, contamination and heterogeneity of both the liquid and solid.[24] Angles less than 90° indicate high wettability, meaning the liquid will easily wet the solid surface under test conditions. For some liquid/solid combinations wetting will occur so completely as to cause an effective contact angle of $\theta = 0°$. An example of this is ethanol on soda-lime glass.[25] For angles greater than 90° the reverse is true and the liquid will not easily wet the solid. Liquid mercury on glass is typically reported as having an angle, $\theta = 148°$.[26] Water on specially prepared Teflon can have a contact angle very near 180°, exhibiting hardly any wetting at all.[27]

In the following we will examine the theory behind wetting behavior and contact angle formation. We begin by defining the underlying principles and forces that cause wetting. We then describe the ideal system and the basic idealized theory that guides contact angle analysis. We will then introduce different factors that can cause deviation from the ideal

and how they effect contact angle and droplet formation. Finally we will relate how the contact angle is significant with respect to electrospray operation.

Polar Covalent Bonds & Dipole Moments

In order to build our description of the mechanisms that drive wetting it is necessary to begin at the most basic and microscopic level. We begin with the intra-molecular forces that form a molecule and effect its movement with respect to other particles. These intra-molecular forces are polar covalent bonds, and the source of molecular movement is the dipole moment.

From basic chemistry we know that atoms bond together to form molecules based on their electronegativity. This is based on electron interactions between them, and if multiple atoms share electrons we say they have formed a polar covalent bond. The resulting molecule will have a three dimensional structure based on electron motion and will have a net positive, negative or neutral charge depending on the nature of those electron interactions. However this net charge is not uniformly distributed within the structure of the molecule and their will be regions of positive or negative charge. These charged regions will have a "center of mass", forming a net positive region within the molecule and a net negative region.[28] Each molecule then forms a dipole that may be asymmetric. As a result, when the molecule is attracted or repelled by other charged particles it will experience a dipole moment, μ, measured in charge multiplied by the distance between charge centers $(C \times m)$. For dipole symmetric molecules μ will be zero, for asymmetric molecules it will be non-zero and greatly influence the motion of the molecule. This is illustrated for two molecules with a non-zero and zero dipole moment respectively in Figure 11.
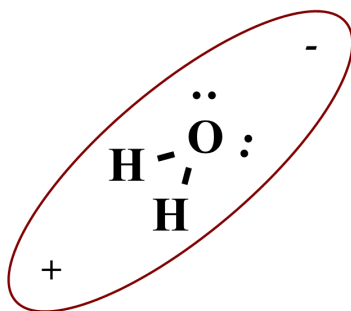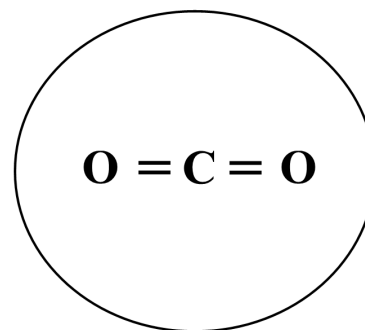
Figure 11: Dipole formation for water (left) and neutral carbon dioxide (right).

14

van der Waal's Forces

We now examine the forces that can occur between multiple molecules in a substance, intermolecular forces. These forces are electrostatic in nature, occurring between unlike charges. There are several different types of intermolecular forces that can act on a molecule, however they are collectively known as van der Waal's forces.[28] This term comes from Dutch scientist Johannes van der Waals who was one of the first to postulate in his 1873 thesis that molecules have a finite size and are attracted to each other by intermolecular forces. There are four types of van der Waals Forces, each of which causes molecules to attract and repel each other when in close enough proximity.

Ion-Dipole & Dipole-Dipole Forces

Each molecule has a net polarity and dipole moment due to the sum of the individual bond dipoles within the molecule previously described. This net polarity will form positive and negative regions in the molecule that can attract oppositely charged ions or oppositely charged regions of other molecules. When this occurs between a molecule and an ion, we call it an Ion-Dipole force. If multiple molecules are attracted to each other we call it a dipole-dipole force. This is shown in Figure 12. The reverse is also true in that dipoles and ions of like charge will repel each other instead of attracting. Ion-dipole forces are very strong compared to other van der Waals forces $\left(10 - 50\frac{kJ}{mol}\right)$, while dipole-dipole forces are typically the weakest $\left(3 - 4\frac{kJ}{mol}\right)$.[28]
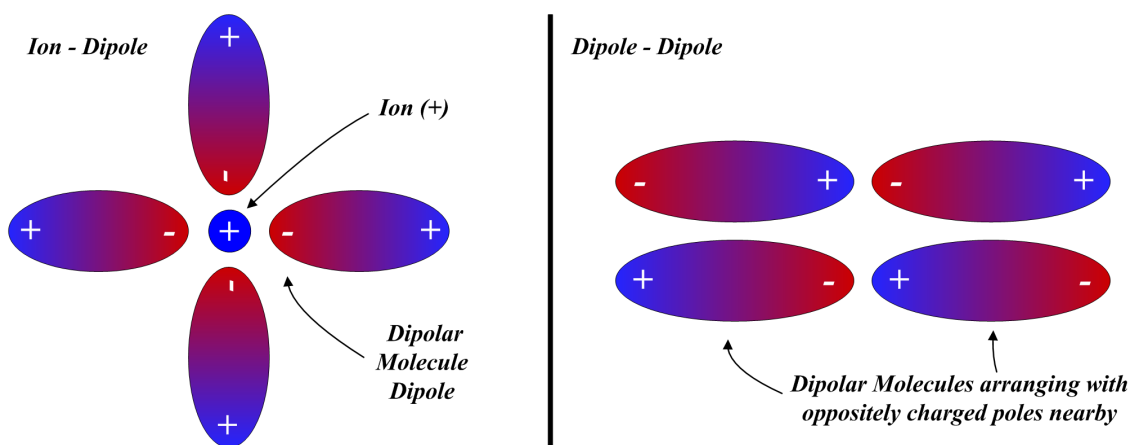
Figure 12: Diagram illustrating ion-dipole (left) and dipole-dipole (right) attraction forces.

London Dispersion Forces

In addition to forces acting only on charged or polar particles, there are also forces that act on all atoms, ions and molecules regardless if they are positively charged, negatively charged or carry no net charge at all. These forces are called the London dispersion forces, named for German-American physicist Fritz London who carried out initial research into intermolecular forces and coined the term "dispersion force". London dispersion forces are a result of the random motion of constituent particles that continuously change the instantaneous charge distribution of a particle. As the charged particles that make up an atom or molecule move they shift the positive and negative charge distribution. At any given instant the charge distribution may be very different and this can cause a constantly changing ion-dipole or dipole-dipole effect even in a molecule or atom that would be considered of neutral charge. This is illustrated in Figure 13. London dispersion forces are very weak, sometimes more so than dipole-dipole forces $\left(1 - 10\frac{kJ}{mol}\right)$.[28]
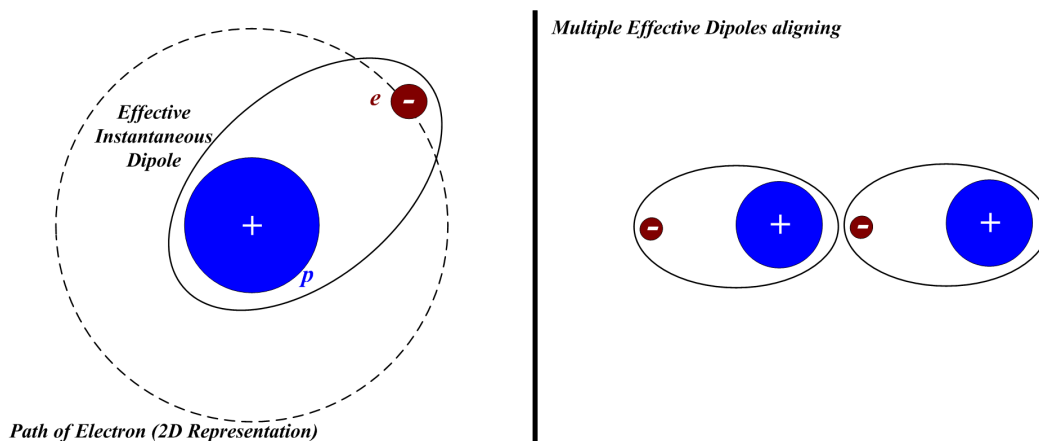
Figure 13: Illustration of the instantaneous dipole formed by electron motion in a hydrogen atom(left) and how these instantaneous dipoles can attract each other(right).

Hydrogen Bonding

Hydrogen bonding occurs when a hydrogen molecule comes in close proximity to an electronegative atom such as oxygen, nitrogen or fluorine that is attached to another molecule. Hydrogen bonding occurs because of hydrogens simple form which allows other molecules within close proximity, allowing strong charge interaction. The unpaired electrons in the electronegative atom form a negative pole while the relatively unprotected proton of hydrogen forms the positive pole. The two are attracted, though this attraction can be affected due to the motion of the hydrogens single electron and that of the electronegative atom. Due to this peculiarity of hydrogen these bonds are unusually strong and are typically as

strong as ion-dipole forces $\left(10 - 40\frac{kJ}{mol}\right)$.[28] A characteristic example of this is the behavior of water molecules which can form extensive hydrogen bonding networks with other water molecules. Because of these strong hydrogen bonds, water has interesting properties such as a higher than typical boiling point than would be expected due to the other van der Waals forces alone.

The Ideal Wetting Model and Young's Equation

Ideal System

In an ideal wetting system there are only three components: a solid, test liquid and surrounding medium, as have been described previously. We assume the solid is smooth ($R_a \approx 0mm$), level, mechanically homogeneous, non-deformable and will not react chemically with the test liquid or surrounding medium. We also assume the liquid to be a stable, chemically homogeneous substance that is non-reactive with the medium or solid. We assume that the medium is an inert gas or liquid that is unperturbed and immiscible with the test liquid. And finally we assume that the temperature and pressure of the system remain constant. Under ideal conditions a droplet of test liquid resting on the solid will form a sphere or spherical cap that is cut off by the plane of the solid, depending upon the amount of wetting. This is depicted in Figure 10. The stable contact angle of this droplet is unaffected by gravity and will always return to the same angle if disturbed. This ideal system would then exhibit only reversible work, with neither friction, plastic deformation or heat generation occurring.[26]

Force Balance

Under ideal conditions the contact angle is a balance between the forces of adhesion, acting across component boundaries between dissimilar molecules, and cohesion, acting internally to each component between like molecules. Adhesion causes the droplet to spread out and wet the solid while, in opposition, cohesion acts to pull the droplet into a spherical shape. We describe adhesion and cohesion more specifically in terms of the surface energy and interfacial energy, both designated γ. Surface energy can be expressed in units of energy per unit area, $\left(\frac{J}{m^2}\right)$, sometimes referred to as the energy density of the materials surface. Surface energy can also be expressed in units of force per unit length, $\left(\frac{N}{m}\right)$, also called the line tension. Surface energy can be defined as the amount of reversible work W_r needed to form a unit section of surface area A of a pure compound. This quantity can be defined mathematically using Equation 1.[29]

$$W_r = \gamma dA \tag{1}$$

There are three surface energy terms that affect contact angle formation. The first being the surface energy of the test liquid in our system. For liquids the surface energy is often referred to as the surface tension. Though this term is applicable to pure liquids, there are misconceptions regarding its use. For the remainder of this discussion, we use the term surface energy instead of surface tension for reasons that will be discussed shortly. We refer to the surface free energy of the liquid using the term γ_{lv}. The subscript lv refers to the fact that the surface energy is both a function of the liquid l and the surrounding medium, often referred to as vapor v. For liquids in an immiscible medium the contribution of the surrounding medium to the surface energy is extremely small and is often neglected.

A simple example of the surface energy exhibited by a liquid is when the calm surface of a standing fluid is deformed by an object without breaking it. This is demonstrated in Figure 14 by "floating" a paper clip on water or by observing water striders, a type of insect, walk across the surface of a calm pool without sinking. By deforming the liquid, its surface area is increased, requiring a specific amount of work to accomplish. In the two examples given the work is done by the weight of the deforming object and the depth to which they deform the surface. A diagram demonstrating this principle can be seen in Figure 15. Surface en-

Figure 14: Demonstrations of liquid surface energy in the real world.

ergy in a liquid is caused by the Van der Waals forces discussed earlier. The molecules of the liquid experience mostly dispersive or hydrogen bond forces (depending on the liquid) resulting in relatively strong cohesion. In an immiscible surrounding medium, molecules at the liquids surface experience negligible forces from the surroundings and much stronger forces from their interior neighboring liquid molecules. The result is that the liquid forms a stable, unbroken, surface. An illustration of this effect is shown in Figure 16. In the absence of wetting or any other forces the liquid will be pulled into a perfect sphere as the van der Waals interactions balance out.

It is important to note at this point that there is a difference between surface energy and surface tension. They are occasionally used interchangeably, generating some confusion. This has arisen because, in pure liquids, the surface tension (defined as the work of stretch-
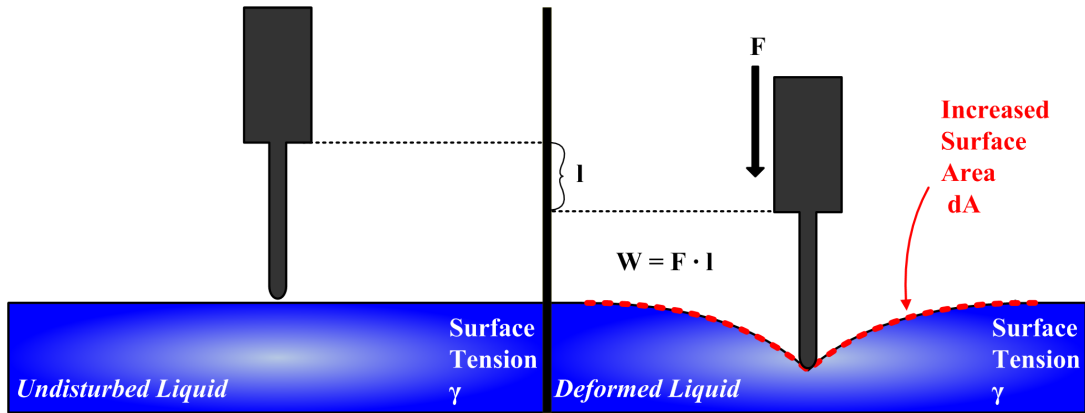
Figure 15: Example of liquid surface energy (surface tension), liquid deformation and the forces involved.
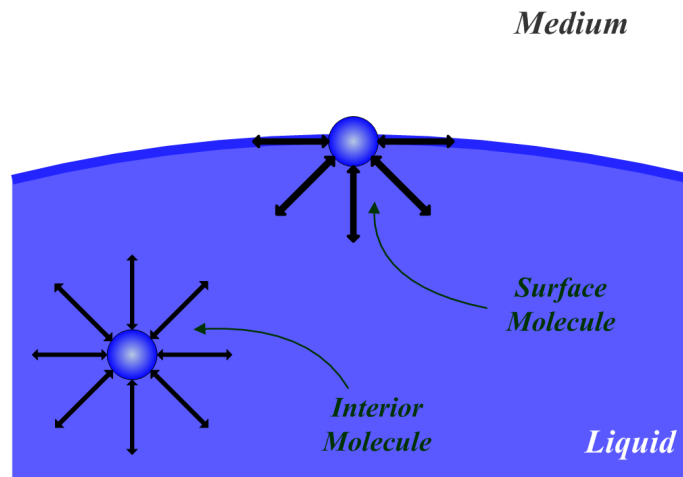
Figure 16: Illustration of how surface molecules in a fluid experience a cohesion force.

ing or deforming a surface) and surface free energy (defined as the work of forming a surface) are both reversible quantities and are equivalent. However for solids, only the latter is associated with reversible work, as stretching a solid surface beyond its yield strength involves irreversible plastic deformation. Thus, for solids, the two terms are not equivalent. For the entirety of this discussion we refer only to the surface energy, as a concept applicable to the work of formation for both solid and liquid surfaces.

The second surface energy term that affects our system is that of the solid. The surface energy for a solid is the amount of work required to form a solid surface area in vacuum. This can be thought of as the amount of energy needed to increase a solid's surface area using a reversible process, like cutting a solid in two or shearing a solid into multiple pieces. We label this surface energy as γ_{s0}. The solid surface energy is defined mathematically by Equation 2.[26] Where G is the Gibb's excess free energy of the solid/vacuum interface, A is the solid surface area, T is the absolute temperature, P the pressure and N_j is the is the

number of excess moles of the jth component.

$$\gamma_{s0} = \left[\left(\frac{\partial G}{\partial A} \right)_{T,P,N_j} \right]_{s0} \tag{2}$$

In addition we define a similar term for the surface energy of a solid surface formed in equilibrium with the saturated vapor of a liquid. We refer to this surface energy as γ_{sv} and define it in much the same way as γ_{s0}. It becomes important later when we relate the surface energy of a solid with, and without, a liquid present. A mathematical expression for γ_{sv} is presented later. For now it can be thought of as the greater or lesser work necessary to form a solid surface area in the presence of a liquid, as opposed to in vacuum.

Unfortunately neither γ_{s0} nor γ_{sv} are easily measured. As described previously these are the amount of energy or work necessary to create or increase the surface area of a solid. It must suffice to say that the surface energy of a solid quantifies the reversible work of forming a unit area of that solid surface. The underlying mechanism of this is also van der Waals forces, which for a solid are much stronger as the molecules of the solid are locked in a rigid matrix.

The third term is that of the interfacial energy between the liquid and the solid, γ_{sl}, when they come in contact and wetting occurs. This interfacial energy is defined as the reversible work of forming a unit area of solid/liquid interface. It is defined by Equation 3, with the same terms as defined in Equation 2, except now with respect to the solid/liquid interface.[26] We can think of γ_{sl} in a similar manner as γ_{lv}, demonstrated in Figure 16. Now instead of molecules at the liquid's surface experiencing greater pull from interior liquid molecules, they experience significant or greater pull from the solid's surface molecules.

$$\gamma_{sl} = \left[\left(\frac{\partial G}{\partial A} \right)_{T,P,N_j} \right]_{sl} \tag{3}$$

The balance between these three energy terms we have defined control the amount of wetting that will occur between the solid and liquid components in the presence of an immiscible medium. The net force of each of these surface energies acting on the liquid can be represented as vectors originating from the three phase boundary (where the solid test liquid and medium meet). These force vectors balance each other under ideal conditions, forming a stable droplet and contact angle. The direction and boundary origin for these forces can be seen in Figure 17.

Young's Equations & Related Terms

Surface and interfacial energy terms and their relationship to the contact angle were originally described in writing by the scientist Thomas Young in the early 1800's. Decades later, thanks to the work of Athanase Dupre and Joshua Gibbs, a mathematical expression
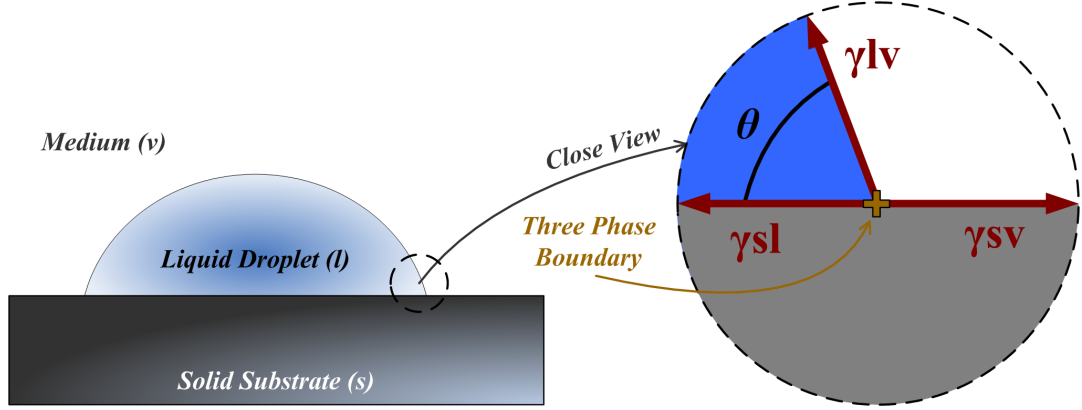
Figure 17: Vectors representing the forces that act on a liquid at the solid/liquid/vapor boundary.

was developed that described the contact angle as a function of these energy terms. This expression is called Young's Equation and is shown in Equation 4.

$$\cos\theta = \frac{\gamma_{sv} - \gamma_{sl}}{\gamma_{lv}} \tag{4}$$

We can see the relationship between Equation 4 and Figure 17. If the surface energy of the liquid γ_{lv} is relatively high, the contact angle will increase as the droplet's cohesive forces cause it to contract on the solid. If the $(\gamma_{sv} - \gamma_{sl})$ term is significantly greater, the adhesive forces between the liquid and solid will cause the droplet to spread out and lower the contact angle.

We now introduce the terms π_{sl} and π_{sv}, known respectively as the adhesion tension[29] and spreading pressure[26]. They are defined in Equations 5 and 6. Because γ_{s0} and γ_{sv} are difficult terms to model or measure we instead view them with respect to other energies involved in the system. The adhesion energy π_{sl} is a measure of the liquids tendency to spread out on the solid. It is directly opposed by spreading pressure π_{sv}. The spreading pressure is the difference between the two solid surface energy terms described in the previous section.

$$\pi_{sl} = \gamma_{s0} - \gamma_{sl} \tag{5}$$

$$\pi_{sv} = \gamma_{s0} - \gamma_{sv} \tag{6}$$

Spreading pressure, the difference between the surface energy of a solid in vacuum and surrounding vapor respectively, is caused by liquid vapor adhesion to the solid surface. The greater this difference, the greater the tendency of the liquid to contract. This can also be described mathematically using the Gibbs adsorption Equation 7.[26] Where Γ_{sv} is the Gibbs surface excess of the vapor on the solid, P is the pressure, P_0 is the vapor pressure of the liquid and R is the gas constant. For low energy surfaces i.e. where $(\gamma_{s0} - \gamma_{sv})$ is small, or experimentally, the contact angle is sufficiently greater than zero, the spreading pressure is negligible: γ_{s0} and γ_{sv} can be considered equivalent. In this case the liquid does not easily adhere to a solid with lower surface energy, resulting in less wetting and a high

contact angle. Using these relationships and Equations we can arrive at Gibbs modified Young's Equation 8.

$$\pi_{sv} = RT \int_0^{P_0} \frac{\Gamma_{sv}}{P} dP \tag{7}$$

$$\cos \theta = \frac{\pi_{sl}}{\gamma_{lv}} \tag{8}$$

Due to these relationships, in an idealized system, we see that wetting is a function of the relative energies of spreading pressure and liquid surface energy. The balance between these forces determines how easily a liquid will wet a solid, and each liquid, solid and medium have both intrinsic properties and interactions that will effect it.

Hysteresis & Advancing/Receding Contact Angles

Having examined the ideal model we now turn to the numerous factors that can add error and irreproducibility to contact angle measurements. These factors are difficult to eliminate, and cause enough uncertainty, to have given contact angle measurements and analysis a "long and tortured history".[26] The primary indication of the uncertainties that occur in a real system is contact angle hysteresis.

It has been generally observed that the contact angle θ_A of a liquid advancing across a solid surface is different than the contact angle θ_R of the same fluid receding from the surface. As we described previously, in an ideal system, the contact angle is stable regardless of perturbations and both θ_A and θ_R should be the same. For real systems this is never the case and θ_A is larger, sometimes much larger, than θ_R. The difference between the two is defined as the contact angle hysteresis H, as can be seen in Equation 9. Most researchers publish advancing contact angles θ_A as an approximation of the ideal contact angle θ previously described.[30]

$$H = \theta_A - \theta_R \tag{9}$$

Hysteresis can be due to surface heterogeneity such as surface roughness or porosity, impurities in the liquid or solid causing uneven surface or interfacial energies, swelling of the solid by the liquid, or a chemical reaction altering both the liquid and solid. Receding contact angles are also typically published to indicate the magnitude of these non-ideal interactions. We describe the more significant of these uncertainties in the following. Advancing and receding contact angles are typically measured using the captive drop technique.[26] In this method the dispensing needle tip is positioned close to the solid and the test liquid is continuously pumped out at an extremely low flow rate. This causes the three component interaction boundary to constantly advance, and the contact angle will typically reach a stable value as the sessile droplet expands. To measure the receding angle the liquid is drawn back into the needle and the resulting liquid angle measured as the liquid contracts. This method is demonstrated in Figure 18.
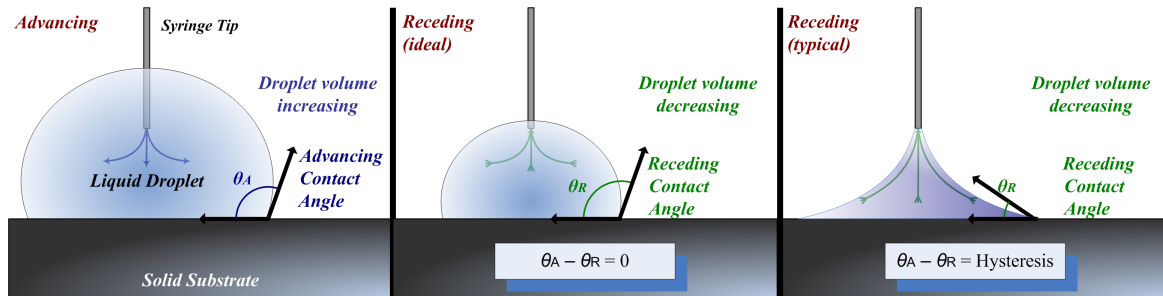
Figure 18: Demonstration of the captive sessile droplet technique.

Surface Roughness

Surface roughness is possibly the greatest source of uncertainty for contact angle measurements. The complexities due to the random nature of surface roughness on a microscopic level make modeling and analysis of its effects extremely difficult. The three component boundary point may be physically impeded from expanding, forming a force imbalance between the surface and interfacial energies. In addition, impurities and small bubbles of the initial surrounding medium may become trapped in small pockets or scratches as the solid is wetted.

It seems that, in response to this uncertainty, many researchers publish surface roughness values for their test solids and then assume in their calculations that the solid is smooth enough to approximate an ideal system. A generalized expression to describe the effects of surface roughness was developed by Robert Wenzel in the early 1900's. This expression describes an "apparent" contact angle θ_W due to surface roughness that is a function of the ideal Young contact angle and the ratio, r_s, of the true surface area of the solid to the apparent area.[31][29] This expression is defined in Equation 10. The net result of surface roughness is that for liquid/solid wetting where the liquid surface energy is the dominant term ($\theta > 90°$), the actual contact angle due to roughness will be greater ($\theta_W > \theta$).[29] The reverse is true for systems where the adhesion tension is the greater term ($\theta < 90°$), the surface roughness will induce more wetting than an equivalent smooth solid ($\theta_W < \theta$).[29]

$$\cos \theta_W = r_s \cos \theta \tag{10}$$

Chemical Reaction & Dynamic Contact Angle Behavior

Under ideal conditions we assume the components of our wetting system to be chemically stable and inert. In reality this is not always the case. Even though the typical signs of a reaction (heat, light, gas generation) may be too small to measure, chemical reactions are known to affect contact angle measurements. Multiple researchers have observed behavior

suggesting minute chemical reactions are occurring between the liquid and solid components during wetting.[26][30] This behavior is exhibited as a dynamic contact angle with respect to time. The droplet will spread or contract slowly over time, causing the contact angle to "wander" asymptotically to a higher or lower value depending on the nature of the reaction. Wang et. al. specifically showed that contact angles between water and several different polymers are not constant with respect to time.[32] Their research with these materials concluded that the contact angle decreases with time for 500 to 2000 seconds depending on the polymer substrate. Their explanation for this behavior involves surface molecular reorganization of the polymer after coming in contact with the test fluid (in this case water).

Though this behavior is an uncertainty in contact angle analysis, it can serve as a useful indication of material contamination. If all three components are shown to be an inert combination, dynamic behavior of the contact angle can indicate a contaminant is present. A characteristic expression for the behavior of contact angles with respect to time, due to chemical reaction, has been developed by Marmur et. al., shown in Equation 11, where A_θ is the base area of the droplet, k and n are empirical coefficients and t is the time from the initial contact between the liquid droplet and the solid.[33] k can be thought of as the initial effective contact angle that will decay as the droplet spreads out at a rate controlled by n.

$$A_\theta = kt^n \tag{11}$$

Effect of Droplet Size

Though it is sometimes assumed that ideal conditions hold and contact angle is independent of droplet size, it has been shown that the advancing contact angle can be a function of droplet volume.[34] It has been suggested by Good & Koo that this occurs for liquids wetting polar solids. They proposed that this behavior is due to inconsistent polar regions in the solid. When the droplet is sufficiently small these inconsistencies will have a relatively large effect on the tensions acting on the droplet. They likened this effect to a negative line tension, acting against the surface energies of the idealized system. They showed that for several liquid/solid combinations that the advancing contact angle would not stabilize until the droplet base diameter reached 0.5 cm.

Other researchers have not posited any explanation for this behavior, other than the observation that advancing contact angles may not stabilize until the droplet has reached a "critical" base diameter, $D_{\theta C}$, of 0.4 to 0.5 cm.[30][31] Criteria for determining whether gravitational effects must be considered have been put forth by Allen in the form of the modified bond number β.[35] The modified bond number is defined in Equation 12, as a ratio of the droplet base radius r_θ and capillary length L_c. The capillary length is defined in Equation 13 where ρ_l and ρ_v are the densities of the test liquid and surrounding vapor respectively and g is gravitational acceleration. Allen states that if the bond number is less

than 1, droplet size effects may be negligible, but if $\beta > 1$ they are not.[35]

$$\beta = \frac{r_\theta}{L_c} \tag{12}$$

$$L_c = \sqrt{\frac{\gamma_{lv}}{(\rho_l - \rho_v)\, g}} \tag{13}$$

Eötvös Model for Liquid Surface Energy

In our description of an ideal system we noted that temperature must remain constant. If the temperature of a real system changes, the surface energies of the components will change and the contact angle will be affected. This is primarily due to variation of the surface energy of the liquid with respect to changing temperature. In order to evaluate the effect on contact angles, this relationship must be quantified. A mathematical expression describing liquid surface energy as a function of temperature was first developed by Loránd Eötvös near the turn of the 20th century. It known as the Eötvös rule and is shown in Equation 14, where V is the molar volume of the liquid, K is a constant of $2.1 \times 10^{-7} J K^{-1} mol^{\frac{2}{3}}$ and T_C is the critical temperature of the fluid.[29]

$$\gamma_{lv} V^{\frac{2}{3}} = K\, (T_C - T) \tag{14}$$

If we substitute the Eötvös rule into Equation 8 we can obtain a relationship for contact angle and temperature. We show this modified form in Equation 15. It must be noted that this equation does not take into account surface energy changes in the solid due to temperature, which may not be negligible.

$$\cos \theta\, (T) = \frac{\pi_{sl}}{V^{-\frac{2}{3}} K\, (T_C - T)} \tag{15}$$

The Critical Surface Energy & Zisman Plots

It was originally observed by Zisman et. al. that when a low surface energy solid is wetted by different liquids, there is a strong linear relationship between the cosine of their advancing contact angles and the liquid's surface energy.[26][29] An example of this phenomena is shown in figure 19, an example of what is called a Zisman plot. This linear relationship, independent of test liquid (with restrictions)[29], implies a constant property of the solid surface. Zisman and his co-workers identified this property as the critical surface tension of the solid, γ_c. This property has since become a standard term for characterizing a solids surface energy. Zisman proposed a function relating contact angle as a function of the liquid surface energy and solid critical surface energy. It is shown in Equation 16, where B is an empirically determined constant typically ranging between values of 0.03-0.04.[29]

$$\cos \theta_Z = 1 - B\, (\gamma_{lv} - \gamma_c) \tag{16}$$

25
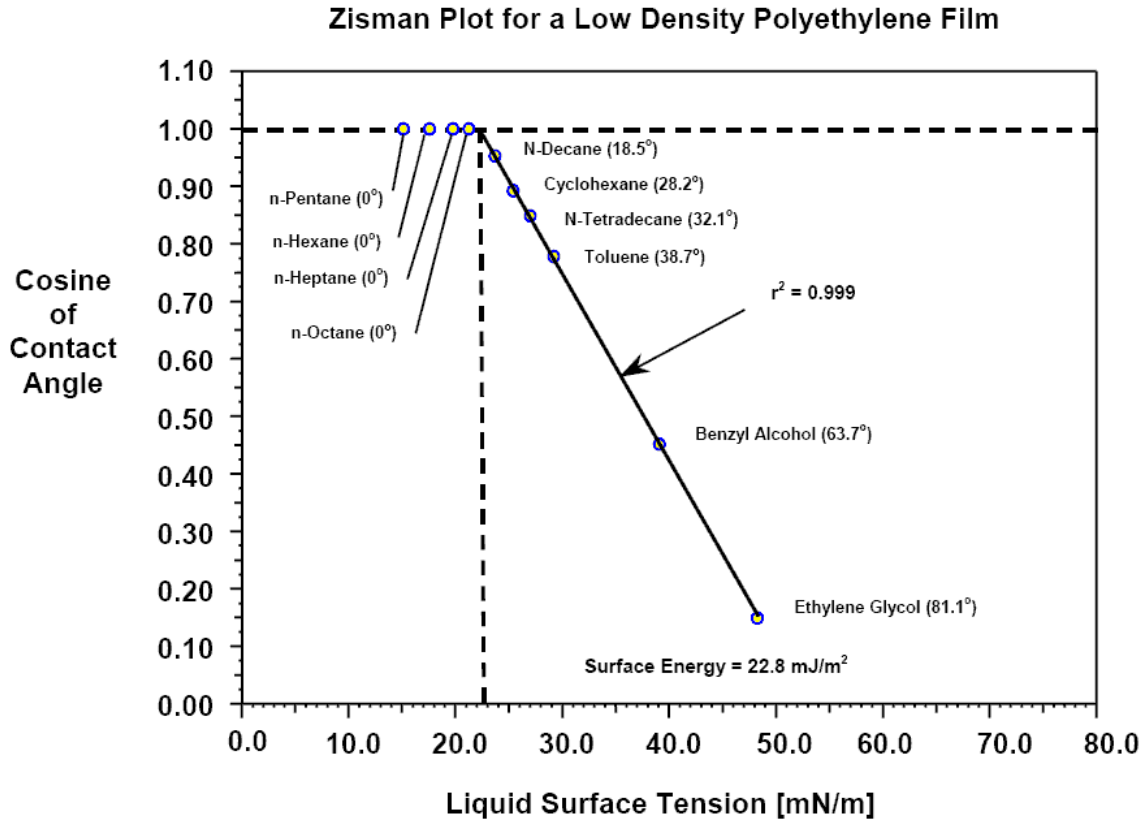
Figure 19: Example of a Zisman plot for a polyethylene film and various test liquids. Figure courtesy of Kruss USA.

Effect of Contact Angle on Electrosprays

Having examined the contact angle and different mechanisms that affect it, we now discuss how the contact angle effects electrospray operation. We find that the most significant effects of contact angle are propellant feed and droplet formation at the emitter tip as well as errant propellant accumulation on emitter grids.

Capillary Propellant Feed

For electrosprays using a capillary feed system, the liquid propellant is not under active pressure and must flow to the emitter tip due to capillary action. Multiple researchers have stated the need for propellant tubing and flow components to be made of materials that are easily wetted by the propellant.[4][5][13][14] This relationship is demonstrated using the Washburn equation shown in Equation 17.[29] It states that the height H to which a liquid will wick in gravity is determined by the contact angle θ, surface energy of the liquid propellant γ_{lv}, pore radius R_p, dynamic viscosity η and time t. We can see that as t approaches infinity, H will stabilize to a single value representing the balance between gravity and the surface tension of the propellant. In a low to zero gravity environment, equilibrium will

26

not be reached until propellant forms a meniscus at the emitter. The Washburn equation then allows us to relate the maximum mass flow rate possible through a feed system, as a function of the contact angle. This becomes important when deciding on materials for the feed system and required propellant flow rates for consistent electrospray operation. As the contact angle decreases, the flow rate of the propellant increases through a capillary.

$$H\left(t\right) = \left(\frac{\gamma_{lv} R_p \cos\left(\theta\right)}{2\eta} t\right)^{\frac{1}{2}} \tag{17}$$

Internally Wetted Emitters

Conroy and Ziemer studied the effect on electrospray performance when contaminant water is present in the EMIIm propellant.[3] The primary consequence of this is water vapor bubble formation in propellant feed lines leading up to the emitter tip. It was demonstrated that the way propellant forms at the tip of the emitter and tip geometry can change the pressure acting on the upstream propellant. They showed that if the resulting pressure is greater than the vapor pressure of the contaminants, bubble formation can be inhibited. They illustrated two examples, state 1 is where the propellant forms a spherical cap at the end of the emitter tip, while in state 2 propellant engulfs the chamfered emitter tip and forms a semi sphere. The geometries of these examples and their significant terms are shown in Figure 20. Equations were developed showing that this induced pressure is a function of the emitter/propellant contact angle, as well as the liquid surface energy of the propellant. Two equations were developed to describe the resulting pressure differential acting on the propellant lines for states 1 and 2, they are shown in Equations 18 & 19 respectively.[3] Where ΔP is the induced pressures, ϕ is the chamfer angle of the emitter tip and r is the radius of bubble formed, which in state 1 is limited by the smaller chamfer diameter. This research showed that in order to reduce the likelihood of bubble formation, emitter tip solid materials or coatings should form a high wetting angle with the propellant.

$$\Delta P = \frac{2\gamma_{lv}}{r_\theta} \sin\left(\theta + \phi\right) \tag{18}$$

$$\Delta P = \frac{2\gamma_{lv}}{r} \frac{\left[1 \mp \cos\left(\theta + \phi\right)\right]^2}{\left[1 \mp \cos\left(\theta + \phi\right)\right]^2 \cos\left(\theta + \phi\right) \tan\phi} \tag{19}$$

Grid Obstruction & Arcing

Problems that have affected electrospray performance have been shorting between the emitter and grid as well as the obstruction of grid apertures due to errant propellant.[5][14] Arcing has typically been due to the presence of excessive propellant at the emitter tip.[6]
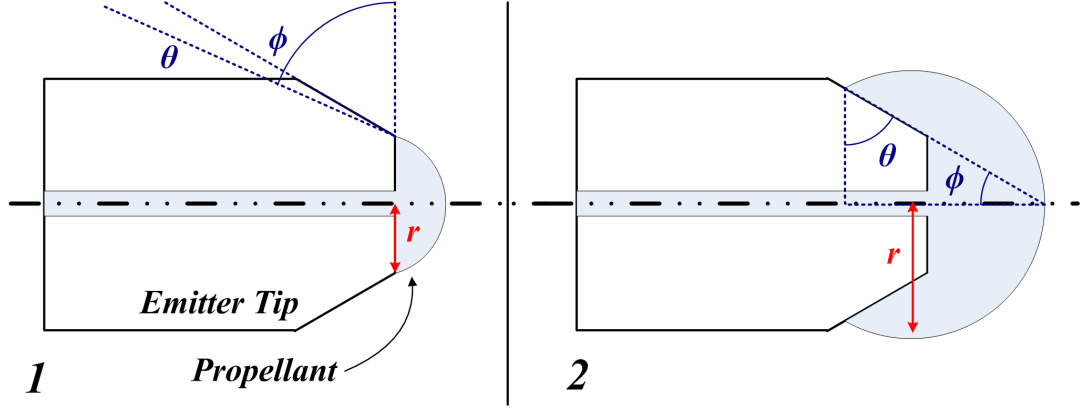
Figure 20: Geometry of chamfered emitter tip and propellant formation.

When electric fields are applied, the droplet of propellant at the tip forms a Taylor cone and, the larger the initial droplet, the longer the Taylor cone will be. If the Taylor cone is sufficiently long it may come in close enough proximity to arc with the grid and either damage the emitter or short the high voltage circuit.

Borrowing from Conroy and Ziemer's work, mentioned previously, we can see how the contact angle might affect this process. For a larger contact angle, a larger volume of propellant will form at the tip. Volume is expressed as a function of contact angle in the two equations below, derived by Conroy and Ziemer. Equation 20 applies to the shallow cap of propellant shown on the left hand side of Figure 20 and Equation 21 corresponding to the large propellant droplet engulfing the tip, shown at the right.[3] Here, r_i is the radius of curvature for the droplet and b is the smaller radius of the chamfered tip. We show the effect of increased volume and how it might lead to closer proximity between the Taylor cone and grid in Figure 21. This shows the contact angle's possible value in inhibiting arcing between the emitter tip and grid.

$$V = \pi \left\{ \frac{2}{3}r_i^3 \mp r_i^2 \sqrt{r_i^2 - r^2} \mp \frac{[r_i^2 - r^2]^{\frac{3}{2}}}{3} \right\} \tag{20}$$

$$V = \pi \left\{ \frac{2}{3}r_i^3 \mp r_i^2 \sqrt{r_i^2 - r^2} \mp \frac{[r_i^2 - r^2]^{\frac{3}{2}}}{3} - \frac{1}{3}\left[r_i^3 \sin^3(\phi + \theta) - b^3\right]\tan\theta \right\} \tag{21}$$

Another failure mechanism for electrosprays is obstruction of the grid due to errant propellant. Occasionally the trajectory of an individual droplet/particle of propellant will become skewed and the droplet will accumulate on the grid instead of passing through. Over time multiple droplets can accumulate, forming a large enough droplet to obstruct the passage of propellant. This effectively destroys one or more emitter/aperture pairs. Over time, if this accumulation has a high propensity for wetting, it could spread to block multiple apertures and adversely effect the overall electrospray performance. This would imply that grid materials or grid coating materials should not be easily wetted by the propellant to help
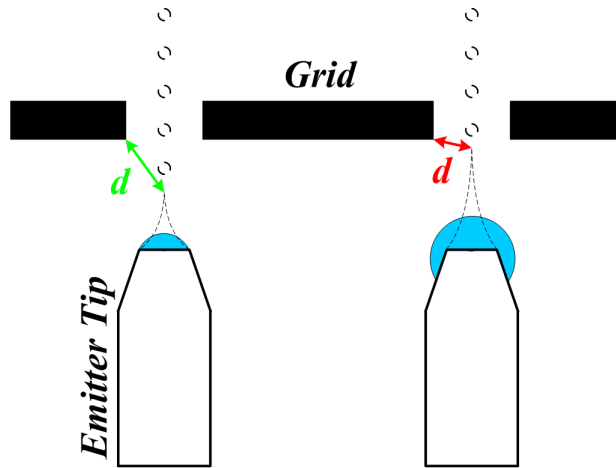
Figure 21: Proximity of Taylor cone to the grid, as a consequence of contact angle.

mitigate this problem. Knowing the contact angles of suitable materials then becomes of importance.
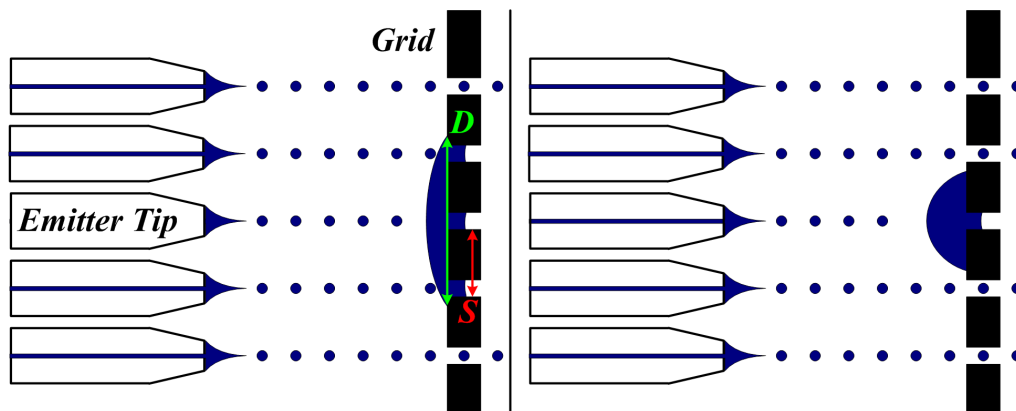

Figure 22: Accumulation of propellant on emitter grid with low contact angle (left) & high contact angle (right).

Results

Measurements were taken between January and October 2011 and consisted of several different approaches to characterizing the wetting of eleven substrates by the commercially available ionic liquid EMIIm. As discussed previously, the primary indicator of wetting is the contact angle, itself a function of the surface energies of EMIIm and the substrate being tested. In the analysis section we illustrated the relationship between contact angle formation and how it pertains to electrospray reliability and performance. This section presents contact angle and liquid surface energy data and attempts to correlate them with underlying mechanisms and principles. Throughout this section we will refer to the effective contact angle θ'. This term represents the actual value measured in this experiment, which is a function of the idealized forces and uncertainties previously discussed.

EMIIm Surface Energy

Early on, a test campaign was carried out to measure the surface energy of the EMIIm obtained and attempt to relate it to ambient conditions, beginning with temperature $\gamma_{lv}(T)$. These tests involved driving the internal ambient temperature of the chamber (at atmospheric pressure) to different values. The temperature of the stainless steel reservoir was also driven to the same temperature. EMIIm was then pumped through the dispense system at a slow flow rate, allowing time for the EMIIm to come to equilibrium temperature in the reservoir. It was then allowed to form a pendant drop (typically 2 μL in Volume) at the syringe tip, which was then recorded and analyzed using the FTA125 software.

The resulting data and corresponding linear curve fits (orange dotted line) establishing EMIIm surface energy as a function of temperature are shown in Figure 23. Each data point taken (shown as orange circles) is an average of twenty separate pendant drop tests taken at the same temperature setting. Also shown in Figure 23 are the same measurements taken on EMIIm in previous work by other researchers using the pendant drop technique[18], and the Wilhelmy Plate method[10][20]. Modeled data calculated using the Eotvos Rule, from Equation 14 on page 25, and published properties of EMIIm listed in Table 1 on page 7 are shown as a dotted black line. Data taken at AFRL agrees fairly closely with other researchers, though relative inaccuracy in the measurement makes the temperature trend less clear. The observed inaccuracy may be due to differences in sample handling and the details of taking measurements using the FTA125. This test showed that the EMIIm obtained for this experiment exhibited the same properties described in contemporary work, measured with similar methods.

Temperature & Pressure

The second portion of this campaign was to determine the effect and magnitude of ambient pressure on EMIIm surface energy, $\gamma_{lv}(P)$. Ideally this measurement would have involved
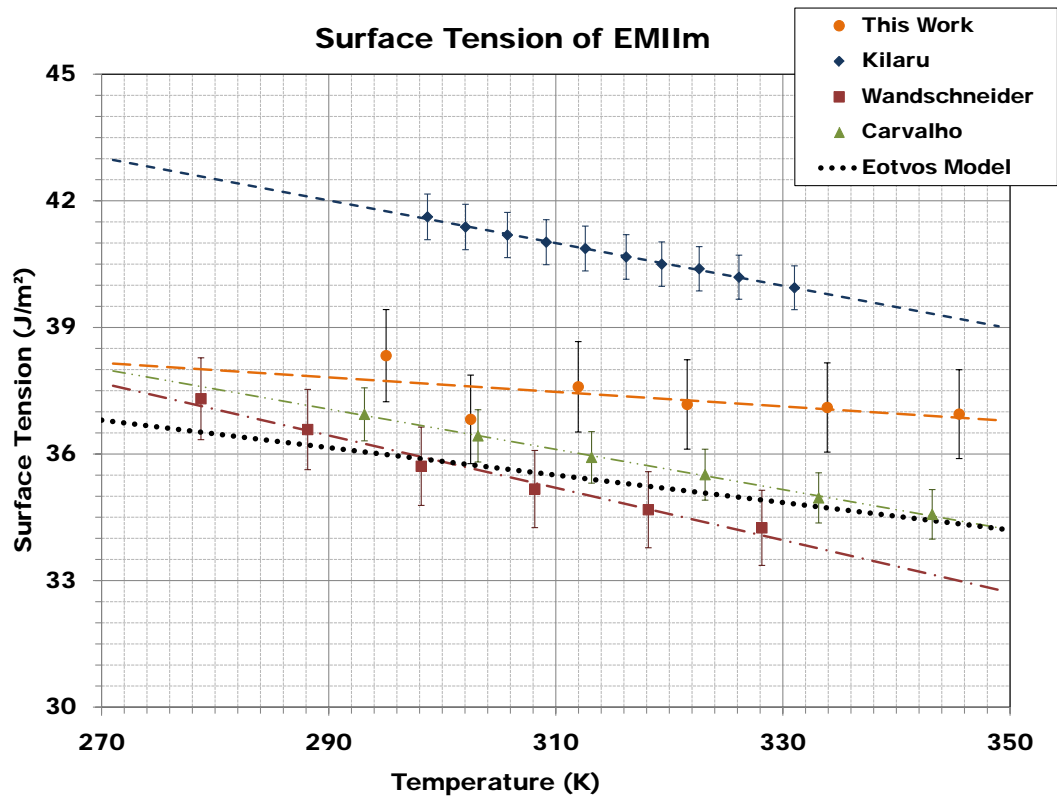
Figure 23: Graph of EMIIm Surface energy (tension) as a function of temperature from this work, the Eotvos model and other researchers.

forming a single pendant drop and then varying the pressure through an entire range from ambient to the lowest pressure (highest vacuum) possible, simulating a space environment. Unfortunately, changing the ambient pressure while a pendant drop was present at the tip of the dispense needle typically resulted in the drop being dislodged or retracted. This was due to air that would inevitably become trapped in the dispense system. When decreasing chamber pressure, the trapped air would expand and push more fluid out. When allowing chamber pressure to rise from low pressures back to ambient the opposite would occur and the droplet would retract into the needle tip. In either case the measurement was interrupted, preventing a single data set taken through a pressure range.

To address this issue, pendant drops were formed and measured at a single pressure for each test. Initially only two pressures were measured, ambient atmosphere (1 ATM, 760 Torr) and the lowest pressure attainable by vacuum Chamber #8 first stage (approximately 40 mTorr). Eight tests were averaged for each pressure and the results showed no noticeable change in surface energy. This indicated that any change occurring in EMIIm surface energy was too small to measure. Additional measurements were then taken where temperature was varied in a similar fashion as the previous test, to see if pressure change would have an effect on the temperature trend. The initial data set (near room temperature, $293K$) and the subsequent extended temperature/pressure data are shown in Figure 24. Each data point in Figure 24 is an average of eight tests. Note that measurements taken at ambient pressure were limited to a maximum temperature of approximately $50K$. Above this temperature the ambient air would transfer enough heat to the FTA125 camera to affect its
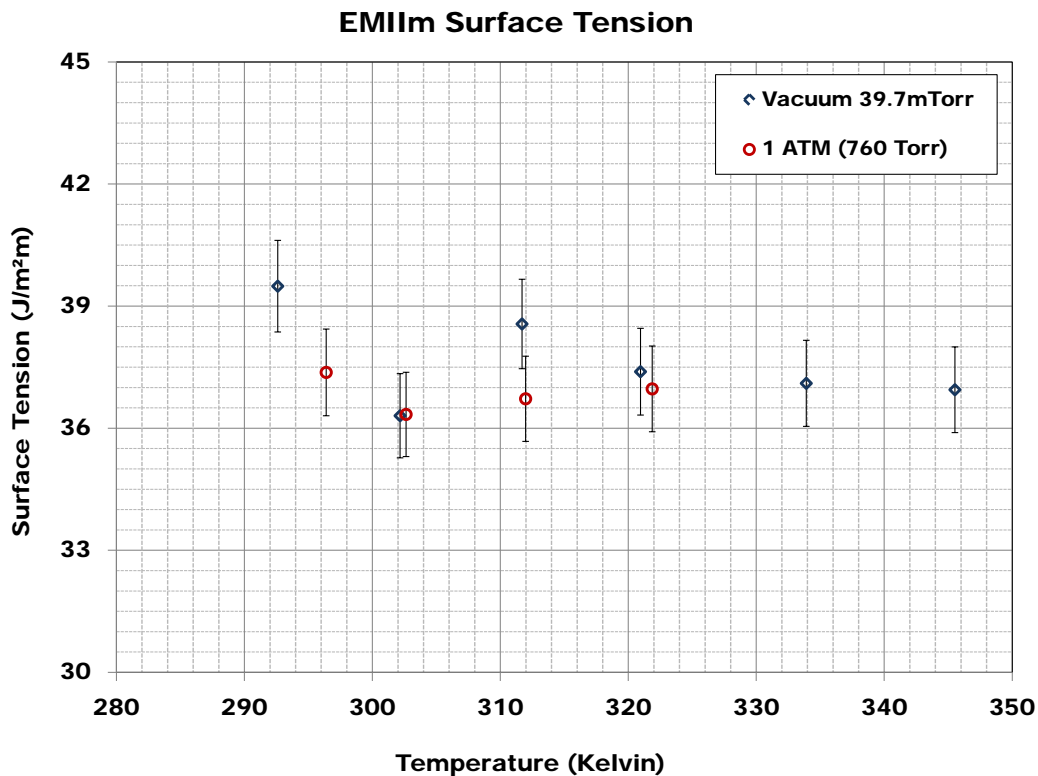
31

Figure 24: Graph of EMIIm Surface energy (tension) as a function of pressure & temperature from this work, the model and other researchers.

operation.

The lack of a clear relationship between EMIIm surface energy and ambient pressure is likely explained by its negligible vapor pressure. One would expect that, as a liquid approaches its critical point, its properties such as surface energy might change significantly. If water had been tested under these same conditions, the change due to pressure would have been drastic as the water would exceed its critical point and vaporize. EMIIm would likely exhibit measurable changes in surface energy as it came closer to phase change, however that transition state (note the critical temperature of EMIm in Table 1 on page 7) would require higher temperatures and lower pressures than this experiment can accommodate. It is likely that some small changes in surface energy were occurring during these test, but are too small to be noticeable against the measurement error.

Equilibrium Contact Angles

The first series of contact angle measurements involved dispensing a single droplet of EMIIm from a short height (approximately 3 mm) above the substrate. When fully formed the droplet would detach from the needle tip and fall to the substrate, wetting it. In these initial "high resolution" tests, data was taken at a frame rate of 10 Hz for a duration of approximately 2 minutes. Initial measurements were taken on mirror finish 316 Stainless
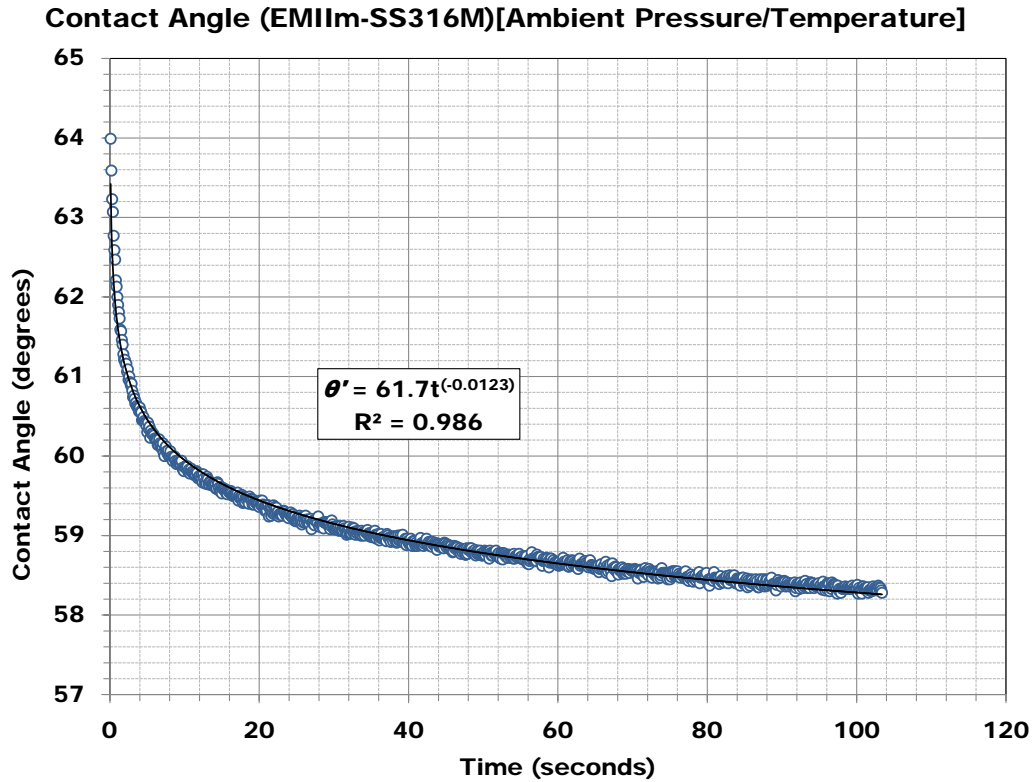
Figure 25: Graph of contact angle formed by EMIIm and SS316M.

Steel, an example test is shown in Figure 25.

Droplet Size & the Bond Number

During these measurements EMIIm droplets consistently detached from the needle tip after reaching a volume of $2.7 \pm 0.2\mu L$. Upon wetting the substrate the average droplet base diameter was 2.2 ± 0.4 (significant deviation was due to contact angle, i.e. the amount of wetting). In order to evaluate whether or not gravitational effects could be neglected it became necessary calculate the characteristic bond number for EMIIm when dealing with droplet of this size. Using these typical droplet dimensions, properties known for EMIIm (See Table 1), and Equations 12 & 13 the modified bond Number was calculated to range between 0.80 and 0.94. This range is below the threshold where gravitational considerations play a part in contact angle formation, according to the theory previously discussed.

Dynamic Angle Behavior

It was immediately noticed that the contact angle did not stabilize to a single value but appeared to decay as a function of time. As the droplet initially struck the surface it would

33

form a high angle and then slowly settle and spread to lower angles following a power law relationship with time. This was eventually recognized as the result of a chemical reaction described by researchers Kwok and Murmur.[30][33] Equation 11, which quantifies this effect, is shown on page 24. A power law curve fitting algorithm was applied using Matlab to obtain coefficient values for K and n from the data. The resulting curve fit line and coefficients are shown over-layed with the measured data in Figure 25.

The causes of this chemical reaction are complex, however it was suggested by Dr. Dean R. Massey that a reaction may have been occurring between the EMIIm and oxide layers formed by many compounds. The oxide itself may have been the source of the reaction, or impurities trapped by microscopic surface imperfections due to the oxide layer. Dr. Massey suggested a procedure he had previously used where strong acid was applied to the substrate surface in order to dissolve the oxide shortly before testing. Some acid was allowed to remain on the substrate surface, in order to prevent new oxide formation, which would vaporize as the chamber pressure decreased. This technique was not used for this experiment for two reasons. The first was that the vacuum pumping system for chamber #8 was not designed to accommodate acidic vapors. The second was the desire to take data on materials representing electrospray components in an actual flight environment. It is not feasible for electrospray components to remain oxidization free before launch or in orbit, therefor taking data on oxidized components was believed to be a more accurate representation of actual operating conditions.
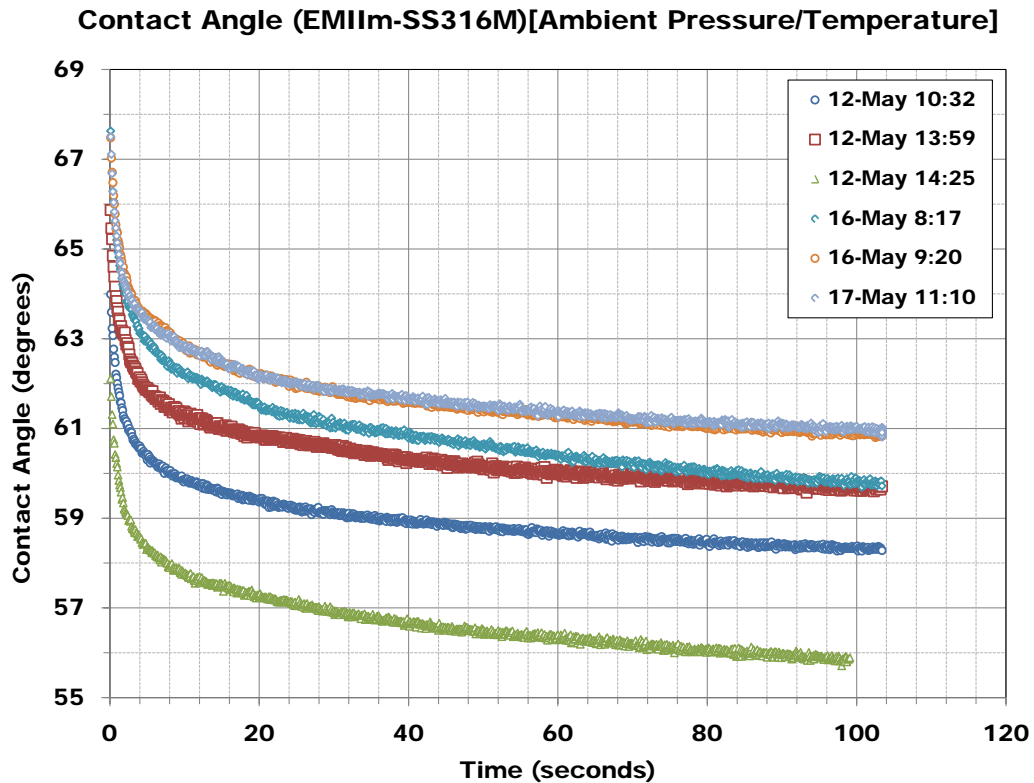

Figure 26: Multiple contact data profiles for SS316M and EMIIm under the same operation conditions.

To verify the repeatability of these time dependant results the same test was performed numerous times on all of the different substrates. Without exception the same behavior was observed for every substrate except PTFE Teflon. Figure 26 shows a typical spread of contact angle profiles taken on the same substrate (SS316M), at the same ambient pressure and temperature. It was noticed that profiles varied greatly in their initial ($t = 0$) distribution, as demonstrated in Figure 26. This variation was problematic as contact angle measurements using the sessile drop technique are generally accepted as having an uncertainty of $\pm$2-3 degrees.[26] Equilibrium measurements taken for this research showed a typical uncertainty of $\pm$5 degrees.
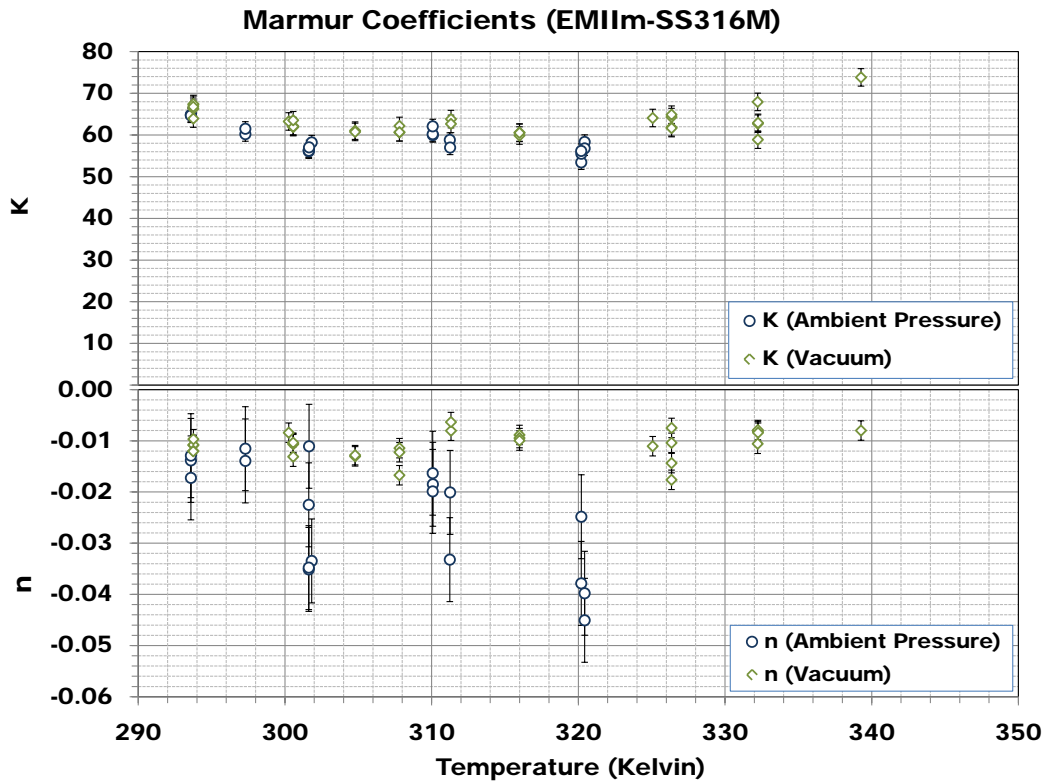
Figure 27: Averaged coefficient data sets for SS316M.

Because this power law trend was likely due to a chemical reaction it was decided to take multiple measurements over a range of temperatures, as was done for surface energy. The purpose behind this was to attempt to demonstrate a relationship between the chemical reaction and temperature. Since the rate of chemical reactions accelerate with increased temperature, it was reasoned that changes in n and/or K due to increased temperature might be evident. Pressure was also varied, producing two data sets, one at atmosphere and under vacuum. Five data points were taken on SS316M at different temperature increments in both ambient atmosphere and vacuum. The resulting data for n and K is shown in Figure 27. We see that there is no clear trend between temperature, pressure and the power law coefficients. n and K remain mostly flat throughout the temperature cycles and there is no apparent difference between measurements taken at atmospheric pressure and in

35

vacuum. This would imply that the changes in the reaction between EMIIm and the oxide layer/contaminants due to temperature or pressure are too small to be measured.

Contaminant Water Removal

It should be noted that prior to this test an attempt was made to vacuum dry the EMIIm as had been described by other researchers.[19][20] Carvalho et. al. described removing water content from EMIIm by placing it under vacuum for 48 hours at a temperature of 353 K under automated stirring. Klomfar used a similar technique on other ionic liquids to remove water, without stirring. It was claimed by both Carvalho and Klomfar that this technique could greatly increase the consistency of contact angle measurements. In an attempt at greater accuracy before the above coefficient/temperature test mentioned was carried out, the EMIIm was placed in a clean petri dish and allowed to sit open to vacuum (approximately 10^{-5} torr) for 40 hours at a temperature of 323 K. Unfortunately no greater accuracy was observed in the subsequent measurements. It was recommended by AFRL chemist Adam Brand that a dry nitrogen titration is the only way to truly dessicate ionic liquids such as EMIIm.
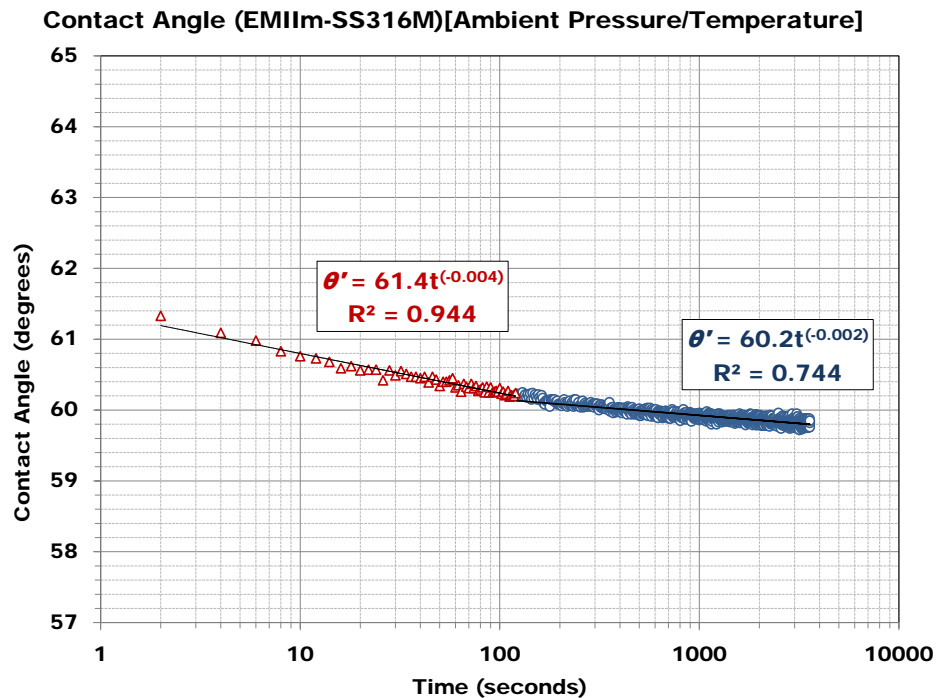
Long Duration Testing

Figure 28: Contact angles taken over one hour on SS316M, note initial transient behavior.

After much review and discussion regarding the data taken at this point the question was asked, what does the contact angle profile look like over a much longer period of time?

36

Does the power law relationship continue on, or does the contact angle stabilize at some point in time and reach equilibrium? In response to this question a longer duration baseline data set was taken on SS316M, over one hour, with a frame rate of $\frac{1}{2}Hz$. The resulting data is shown in Figure 28, note the time axis is now on a logarithmic scale. An interesting feature of this data was a change near 120 seconds, when the decay of the droplet angle appears to transition from one power law function to another. The first two minutes of wetting contact came to be viewed as a transient period, after which the data appeared to form a stable power law relationship. These measurement parameters came to be the standard method used to record equilibrium contact angles. All further contact angle profiles were recorded at similar frame rates, for at least one hour. Power law coefficient fits were now calculated excluding the transient first two minutes of data. Contact angle profiles were subsequently measured for each substrate and the coefficients calculated. These profiles are shown in Figures 29-39.

Contact Angle (EMIIm-Silicon)[Ambient Pressure/Temperature]

$\theta' = 56.4t^{(-0.0106)}$

$R^2 = 0.986$
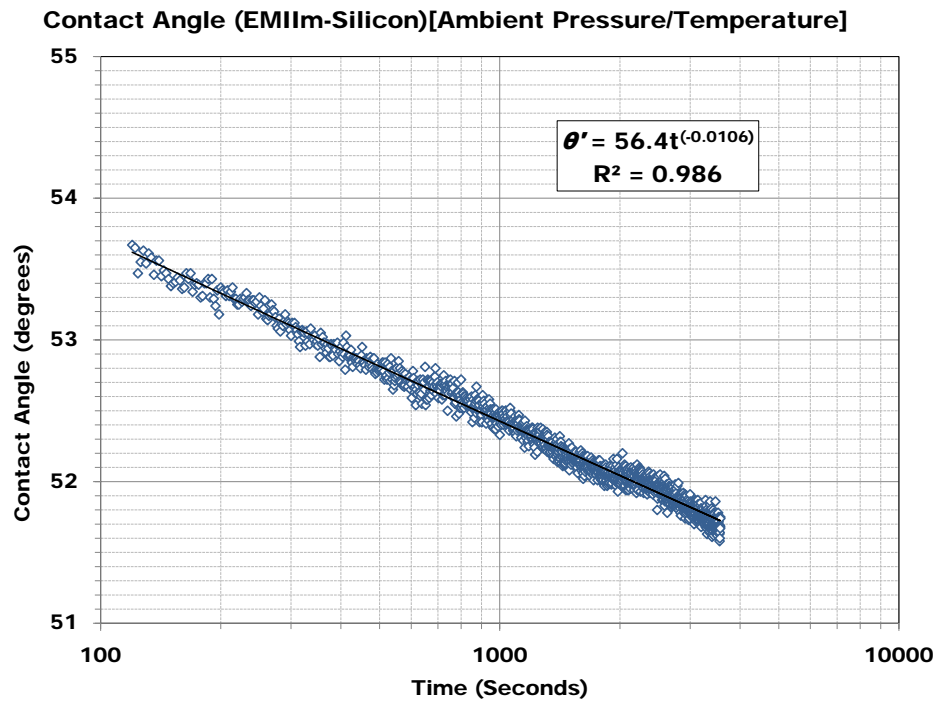
Figure 29: Long duration test on Si, ambient conditions.

37
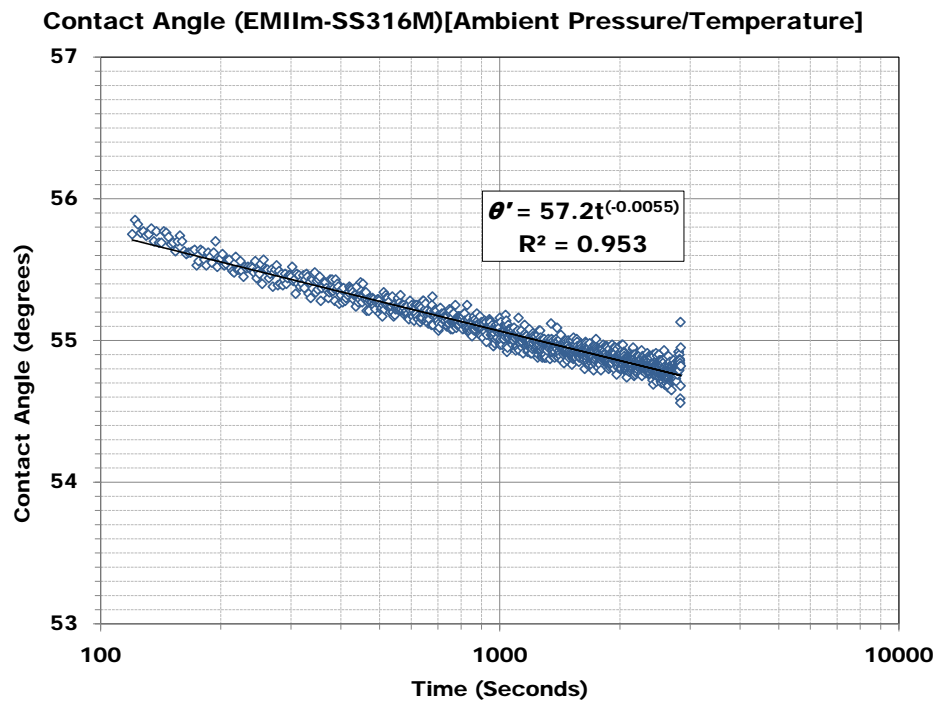
Figure 30: Long duration test on SS316M, ambient conditions.
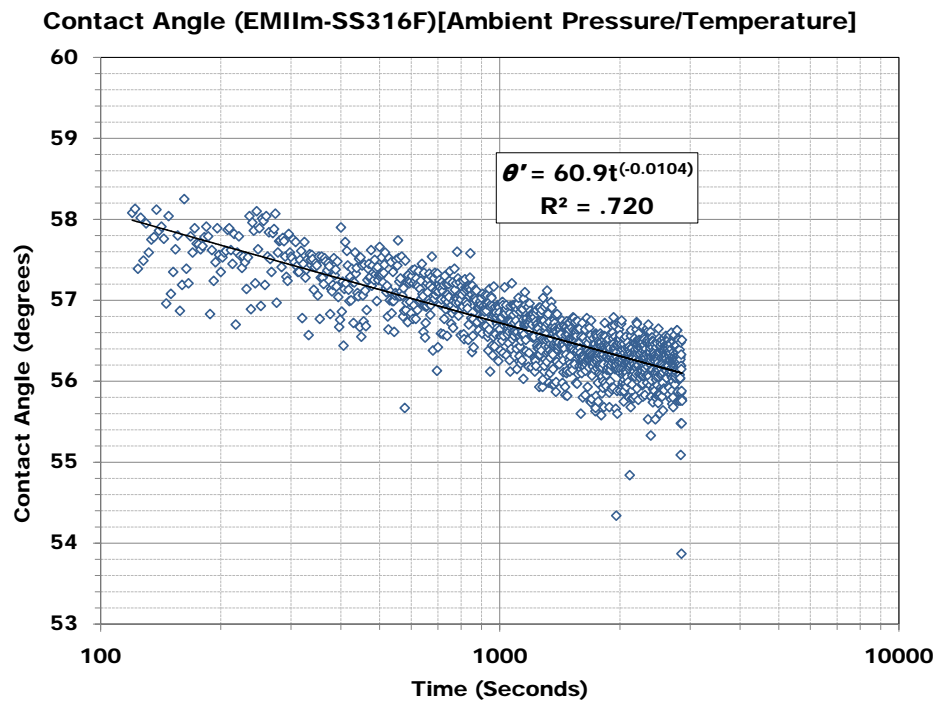
Figure 31: Long duration test on SS316F, ambient conditions.

Contact Angle (EMIIm-SS316C)[Ambient Pressure/Temperature]

$$\theta' = 55.1t^{(-0.0285)}$$
$$R^2 = 0.997$$
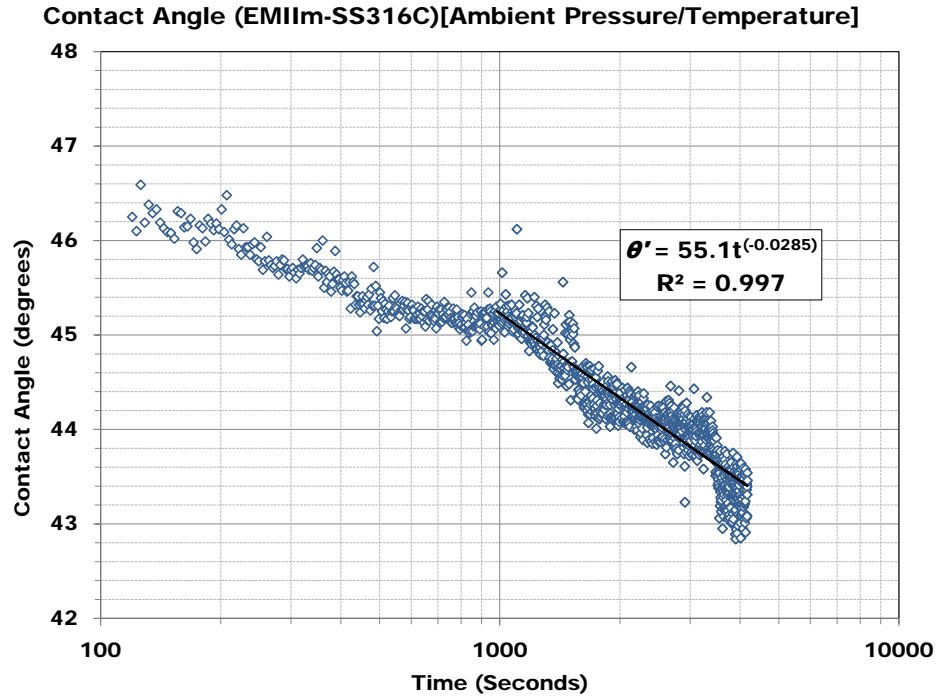
Figure 32: Long duration test on SS316C, ambient conditions.

Contact Angle (EMIIm-Ti)[Ambient Pressure/Temperature]

$$\theta' = 59.3t^{(-0.0079)}$$
$$R^2 = .954$$
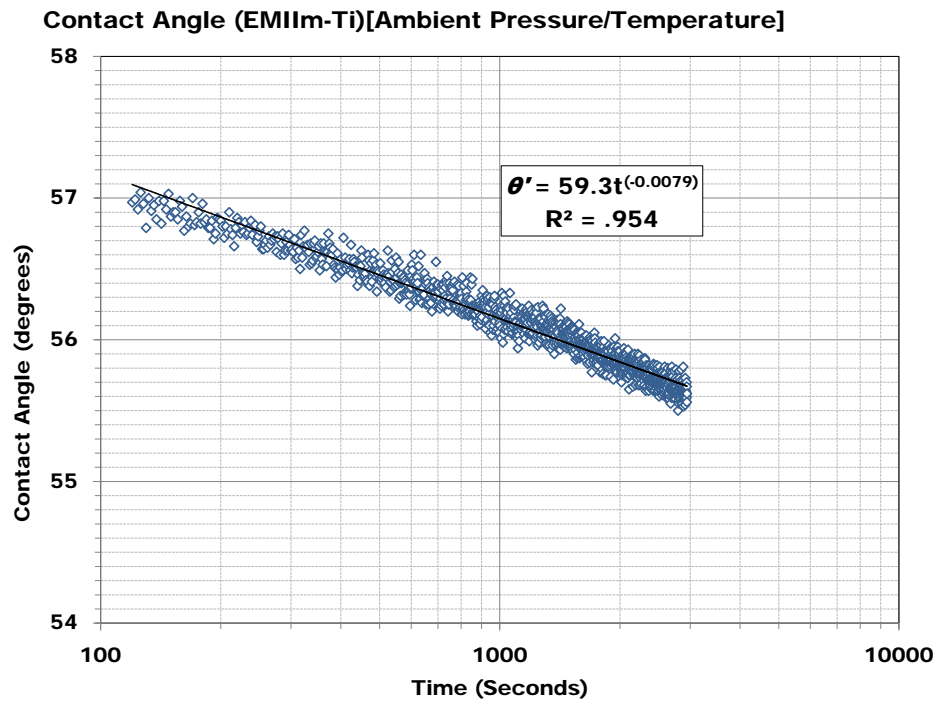
Figure 33: Long duration test on titanium, ambient conditions.

Contact Angle (EMIIm-W)[Ambient Pressure/Temperature]

$\theta' = 39.1t^{(-0.0015)}$
$R^2 = .439$
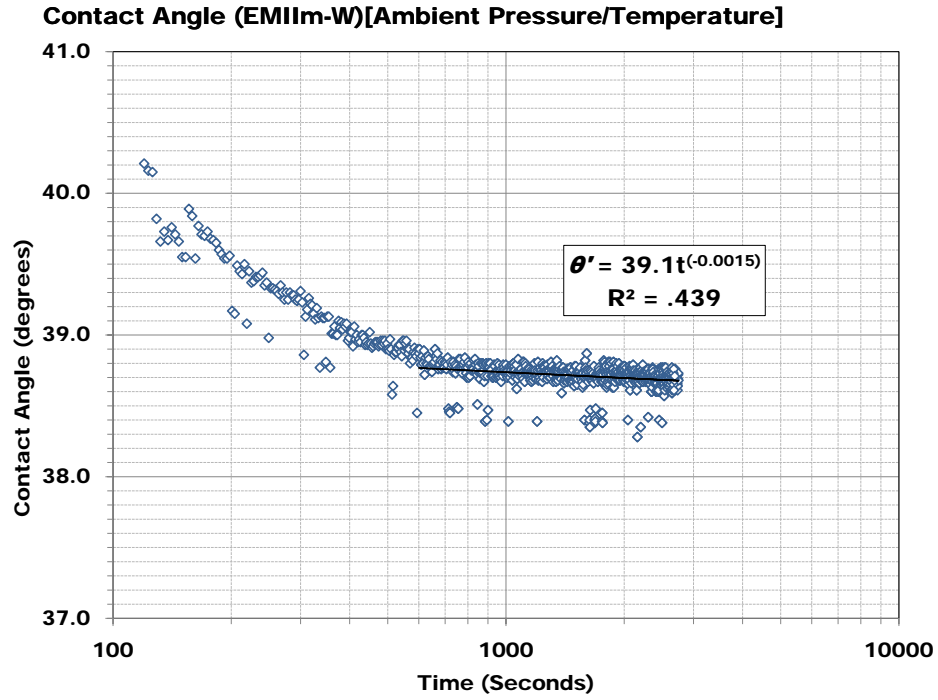
Figure 34: Long duration test on Tungsten. Note unusual, longer, transient period than normal.

Contact Angle (EMIIm-Silica)[Ambient Pressure/Temperature]

$\theta' = 57.9t^{(-0.0281)}$
$R^2 = .997$
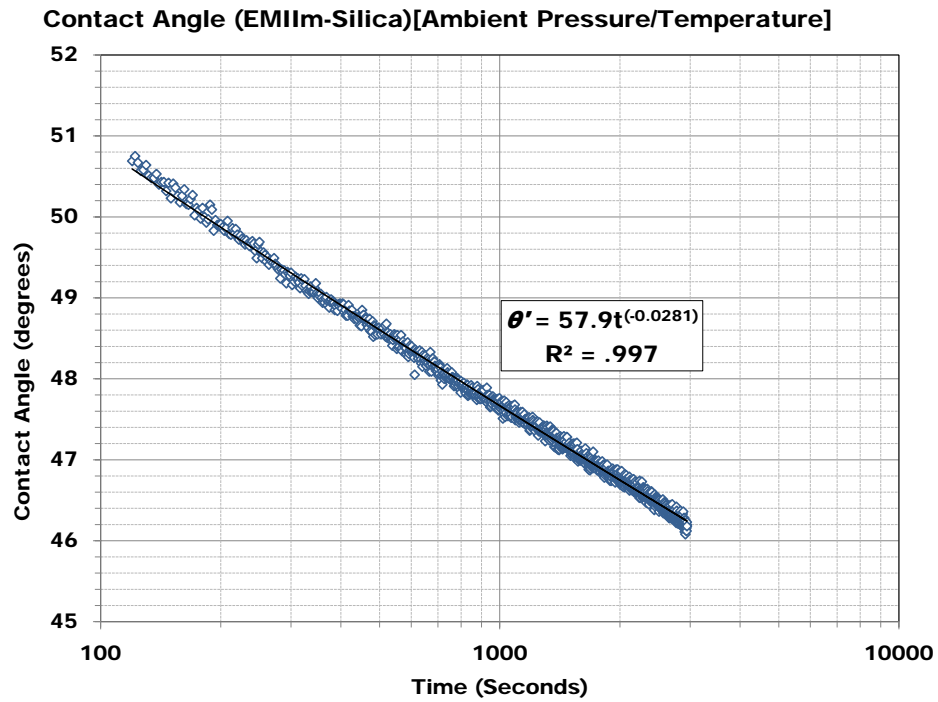
Figure 35: Long duration test on fused silica, ambient conditions.

Contact Angle (EMIIm-Pyrex)[Ambient Pressure/Temperature]

$$\theta' = 45.8t^{(-0.0336)}$$
$$R^2 = .944$$
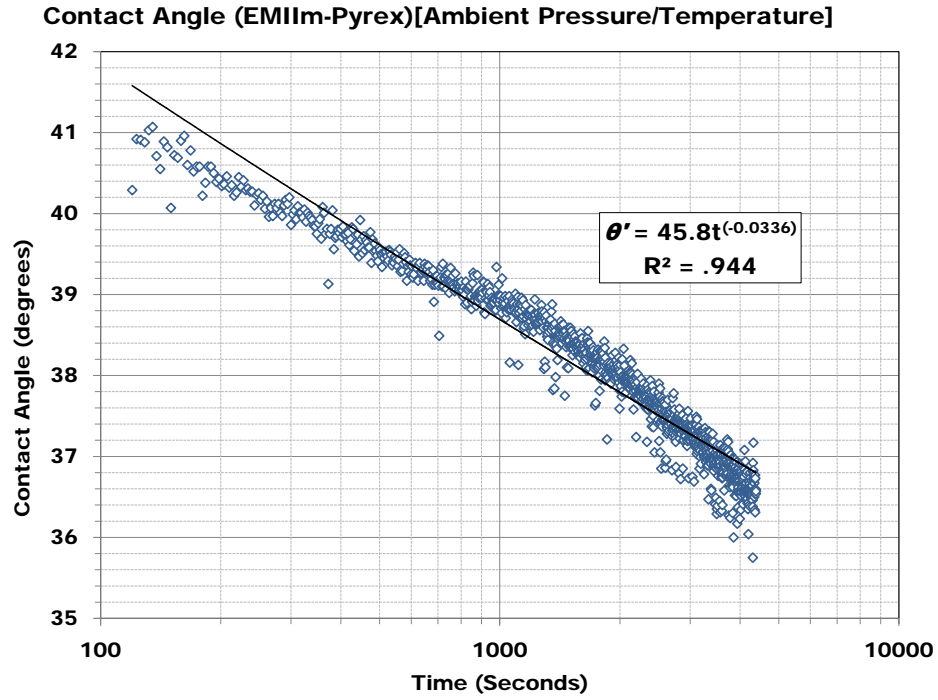
Figure 36: Long duration test on Pyrex, ambient conditions.

Contact Angle (EMIIm-Kapton)[Ambient Pressure/Temperature]

$$\theta' = 59.3t^{(-0.0079)}$$
$$R^2 = .954$$
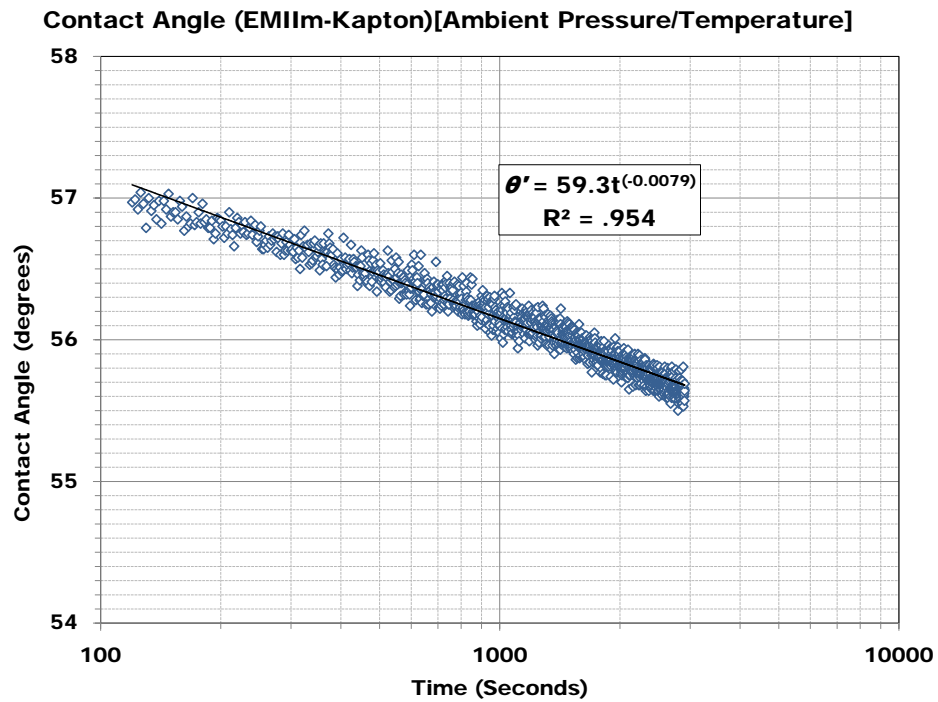
Figure 37: Long duration test on kapton, ambient conditions.

Contact Angle (EMIIm-Glass)[Ambient Pressure/Temperature]

$$\theta' = 45.6t^{(-0.0014)}$$
$$R^2 = 0.714$$
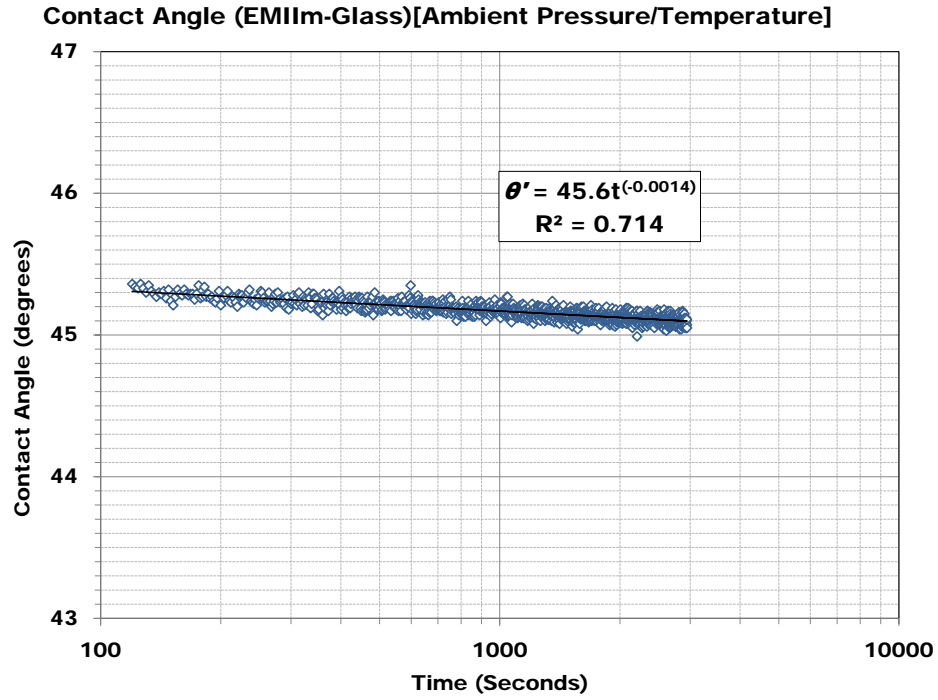
Figure 38: Long duration test on Glass, ambient conditions.

Contact Angle (EMIIm-PTFE)[Ambient Pressure/Temperature]

Legend:
- 11-Jul 9:07
- 11-Jul 11:57
- 11-Jul 17:03
- 13-Jul 8:44
- 15-Sep 12:17

$$\theta' = -5e^{-4}t + 77.3$$
$$\theta' = 2e^{-5}t + 75.9$$
$$\theta' = -2e^{-4}t + 68.3$$
$$\theta' = 3e^{-5}t + 68.2$$
$$\theta' = -8e^{-5}t + 63.1$$
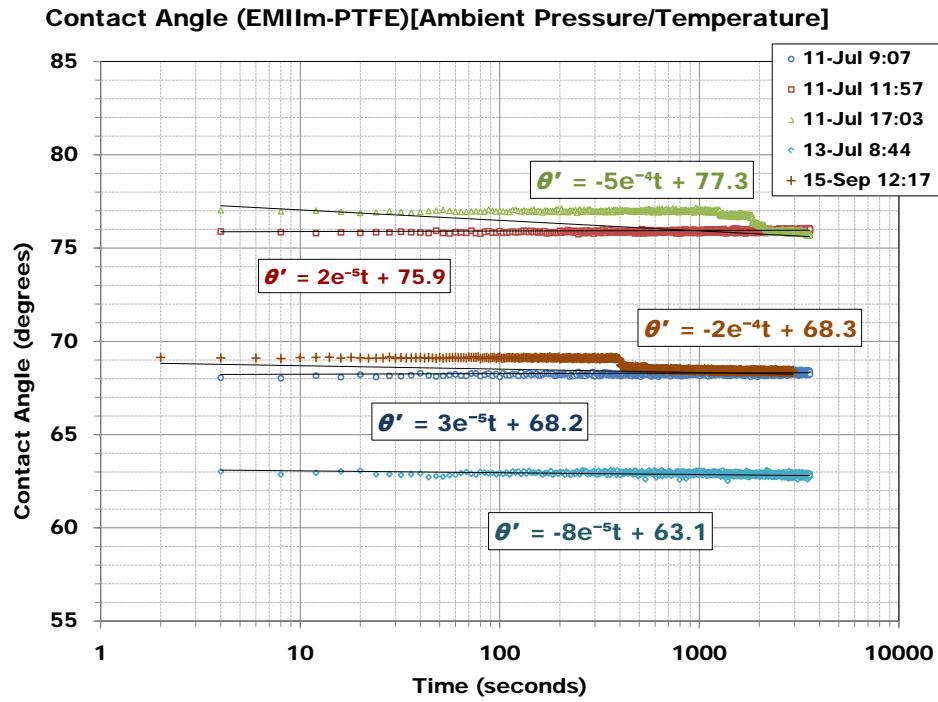
Figure 39: Long duration test on PTFE, ambient conditions.

Table 3: Equilibrium Angle Coefficients

Substrate	k	n	R^2
Fused Silica	57.9	-0.0281	0.99
Soda Lime Glass	45.6	-0.0014	0.71
Kapton	59.3	-0.0079	0.95
Pyrex	45.8	-0.0336	0.94
Annealed Titanium	63.2	-0.0547	0.98
Unsintered Tungsten	39.1	-0.0015	0.44
Undoped Silicon	56.4	-0.0106	0.99
Stainless Steel 316 R_a 0.6	57.2	-0.0055	0.95
Stainless Steel 316 R_a 1.2	60.9	-0.0104	0.72
Stainless Steel 316 R_a 2.5	55.1	-0.0285	0.99
	m	b	R^2
PTFE Teflon	$2 \cdot 10^5$	75.87	0.873

These data sets show a wide range of initial wetting angles, K, and spreading rate terms n. The values for each substrate are listed in Table 3. In theory K should be inversely related to the surface energy of the solid γ_{sv} as we showed previously, see page 20. This behavior is demonstrated in some cases, such as glass exhibiting a much lower K value than teflon (see Figures 38 & 39). Basic Soda-Lime glass has a surface energy over three times greater than Teflon, which is why glass is so easily wetted while Teflon is not. However much of the data did not follow this theory, for instance the tungsten substrate had the lowest k value even though most metals exhibit mid-range surface energy. This is likely due to contamination, vibration or other adverse effects. It can also be seen that k values for the three stainless steel 316 substrates of differing roughness did not form a trend with respect to k. However they did trend with respect to the spreading term n. This trend indicated that increased surface roughness corresponded with a decrease in n, implying a faster rate of wetting/spreading. This agrees with the theory concerning surface roughness and wetting previously discussed, see page 23.

PTFE Behavior

The only substrate to not follow the power law trend was PTFE Teflon. Teflon produced extremely flat/linear contact angle profiles that converged to a single equilibrium value immediately. Coefficients referred to in Table 3, m and b, are the corresponding coefficients of a linear curve fit. This behavior was not the only way in which Teflon stood out among the substrates tested. Teflon tended to develop an electrostatic charge. The EMIIm droplets were influenced by this charge and would behave oddly in close proximity. This behavior first manifested as EMIIm formed a pendant drop at the needle tip. The EMIIm could be attracted by the charged substrate surface and discharge too soon, forming extremely small sessile droplets too small to measure. The EMIIm was also occasionally repelled by the substrate, distorting the pendant droplet as it formed. When finally dispensed the repelled droplet would sometimes fly sideways, out of view, attracted away by an oppositely charged

region. A droplet captured in the act of repelled distortion is shown in Figure 40. Once dispensed the droplets were likely to slide between regions of opposed charge and shift out of focus. A few such drops are seen in Figure 40. No effective countermeasure was found for this behavior and data was taken when surface charge of the Teflon happened to be neutral enough to dispense droplets normally.
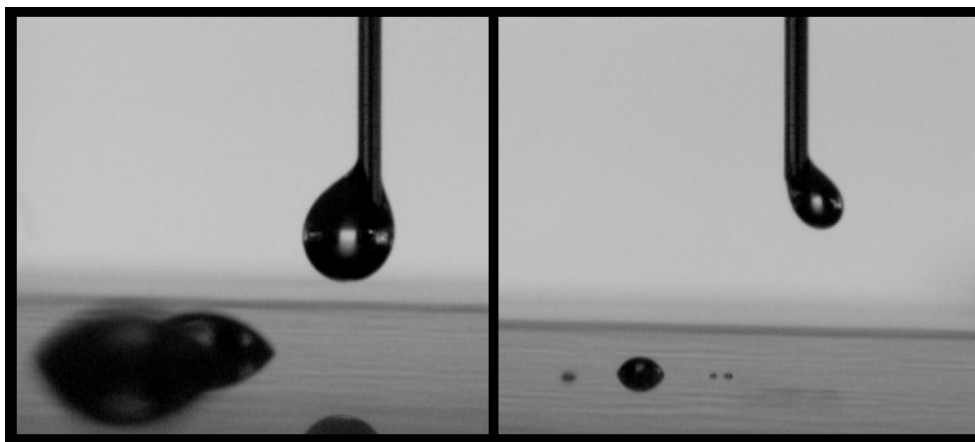

Figure 40: EMIIm behaving strangely during droplet formation due to nearby PTFE surface charge.

Dynamic Angle Behavior Revisited

Having shown the usefulness of taking data over a longer period of time, a second series of measurements attempting to characterize the reaction coefficients with respect to temperature was made. It was believed that longer duration testing, and exclusion of the 120 second transient period from the fit algorithm, would produce more reliable results and be more likely to reveal n and K as a function of temperature. This time, instead of testing on SS316M, Silicon (Si) was used. The silicon substrate exhibited the same power law trend as SS316M, but had a significantly smoother surface (smaller R_a value, See Appendix A). A smoother substrate was seen as likely to yield more accurate results.

Coefficient data for Si is presented in Figure 41, taken at atmospheric pressure. Again the results proved inconclusive, n and K showed no clear dependence on temperature. In theory any chemical reaction or thermodynamic process taking place must be affected by temperature and pressure, but it was not in evidence here. It may be the case that the amount of uncertainty in this measurement makes it difficult to see dependence on temperature. There was no value seen in taking additional data sets under vacuum, consequently only temperature was varied in future testing, while pressure was allowed to remain at ambient.
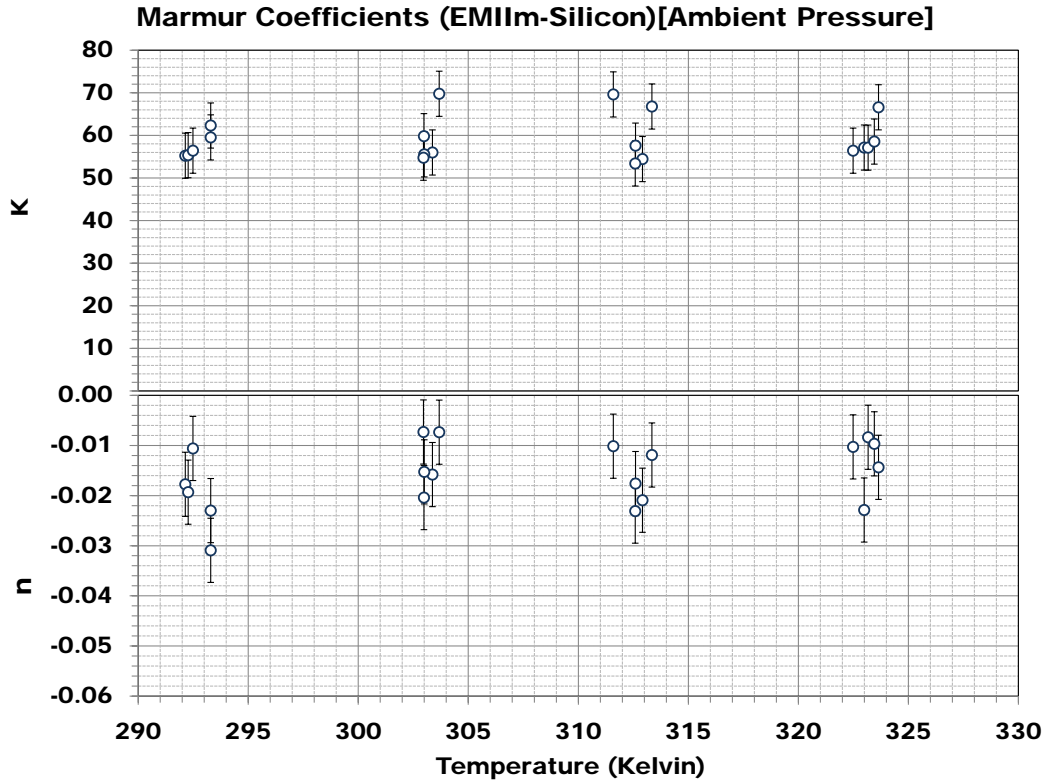
Figure 41: Averaged coefficient data sets for Si.

Equilibrium Temperature Change

It was noticed during testing that if the ambient temperature of the experiment changed in the middle of a test due to lab air conditioning or other causes, the contact angle would also show a slight change. An effort was then made to characterize this behavior. Though too small a difference to measure between consecutive droplets dispensed at different temperatures, it was measurable while measuring the contact angle of a single droplet undergoing temperature change. Testing was then carried out by dispensing a single droplet and allowing it to rest on the substrate for 2 hours. Substrate temperature was then ramped and contact angle data recorded. The most striking response from these tests is shown in Figure 42. We can see that as the temperature of the glass substrate was repeatedly ramped from $280K$ to $327K$, the contact angle oscillated approximately 2 degrees. This can be attributed to changes in both the surface tension of EMIIm and the adhesion tension, a function of the solid. If we use Equation 4 to calculate the relative change in γ_l as a function of θ (assuming π_{sl} to be constant) we see that a 2 degree shift in contact angle should correspond to a $1.4 \ (mNm^{-1})$ shift in surface tension. Using the Eotvos model shown in Figure 23 we see that the idealized shift for the same temperature change is approximately $1.5 \ (mNm^{-1})$, showing close agreement with our measurement.

What is interesting to note is that not all substrates followed the same trend theory. Some substrates tested (Soda-Lime Glass, Tungsten , SS316M/F/C , Silicon, Pyrex, PTFE)

showed increased contact angle with rising temperature, while others (Ti, Fused Silica, Kapton) showed decreasing contact angle with rising temperature. The ideal theory states that as temperature increases, EMIIm surface energy decreases (verified previously). According to the modified Young's Equation 8, contact angle should decrease with increasing surface energy (assuming the adhesion tension remains constant. However during this research it was seen that contact angles on most of the substrates tested actually increased, as shown in Figures 42 and 43, with increasing temperature and likewise decreased and as the substrate temperature was reduced. This would indicate that factors other than surface tension are taking effect during temperature changes. It is possible that the forces represented by the adhesion tension term, π_{sl}, do not remain constant with changing temperature and have an effect.
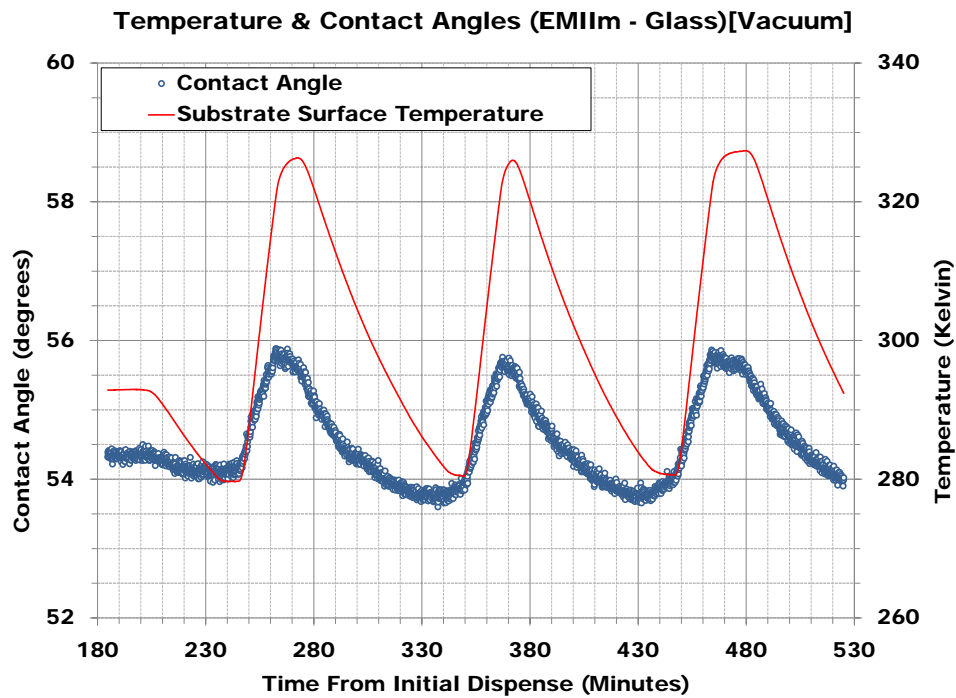
Figure 42: Example of contact angle relationship with temperature, taken on glass.

46
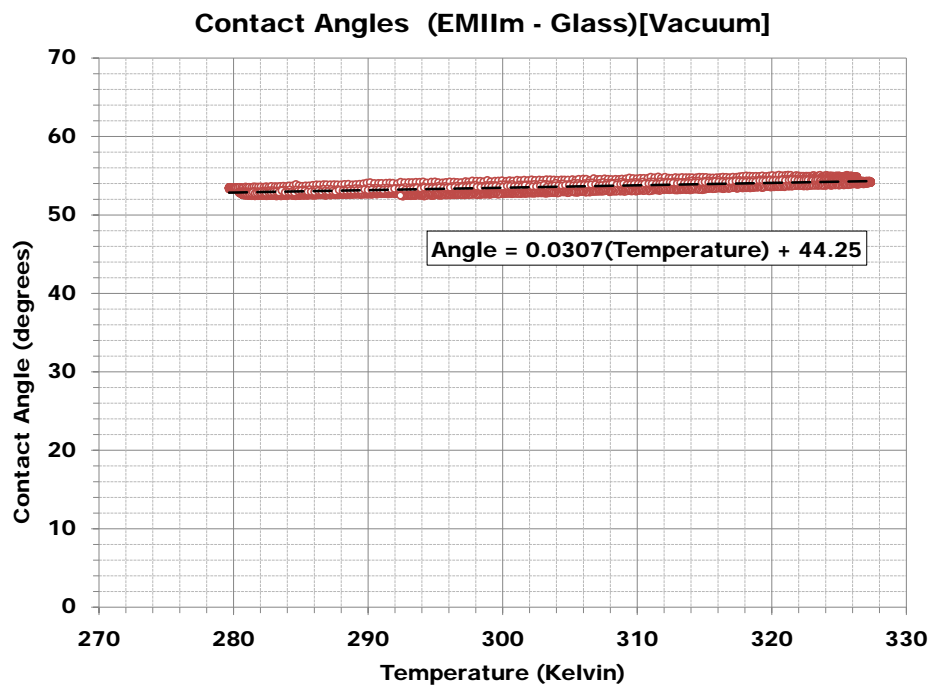
Figure 43: Temperature effect on equilibrium contact angles formed with glass.

Table 4: Advancing and receding angles measured for each substrate.

Substrate	θ_A	θ_R
Fused Silica	51.6	0
Soda Lime Glass	55.2	0
Kapton	52.3	0
Pyrex	49.6	0
Annealed Titanium	52.3	0
Unsintered Tungsten	43.8	0
Undoped Silicon	48.0	0
Stainless Steel 316 R_a 0.63	52.1	0
Stainless Steel 316 R_a 1.2	58.2	0
Stainless Steel 316 R_a 2.5	55.9	0
PTFE Teflon	68.3	56.6

The final data sets taken were advancing and receding contact angles for each substrate. As previously described, advancing values should be closest to the ideal contact angle θ, and H should be 0 for an ideal system. Testing revealed that the only data set that appeared close to ideal was Teflon, which exhibited both constant advancing and receding angles. This can be seen in Figure 45. A more representative data set is shown Figure 44, taken on fused silica. Droplet volume/diameter increases and the contact angle stabilizes to a single value. When retracting fluid most of the substrates demonstrated significant adhesion tension. Instead of receding cleanly, the droplet adhered to the surface, approaching a contact angle of zero degrees. This is likely due to surface heterogeneity of the substrates, or due to chemical reaction. Advancing and receding values for each substrate are listed in Table 4.
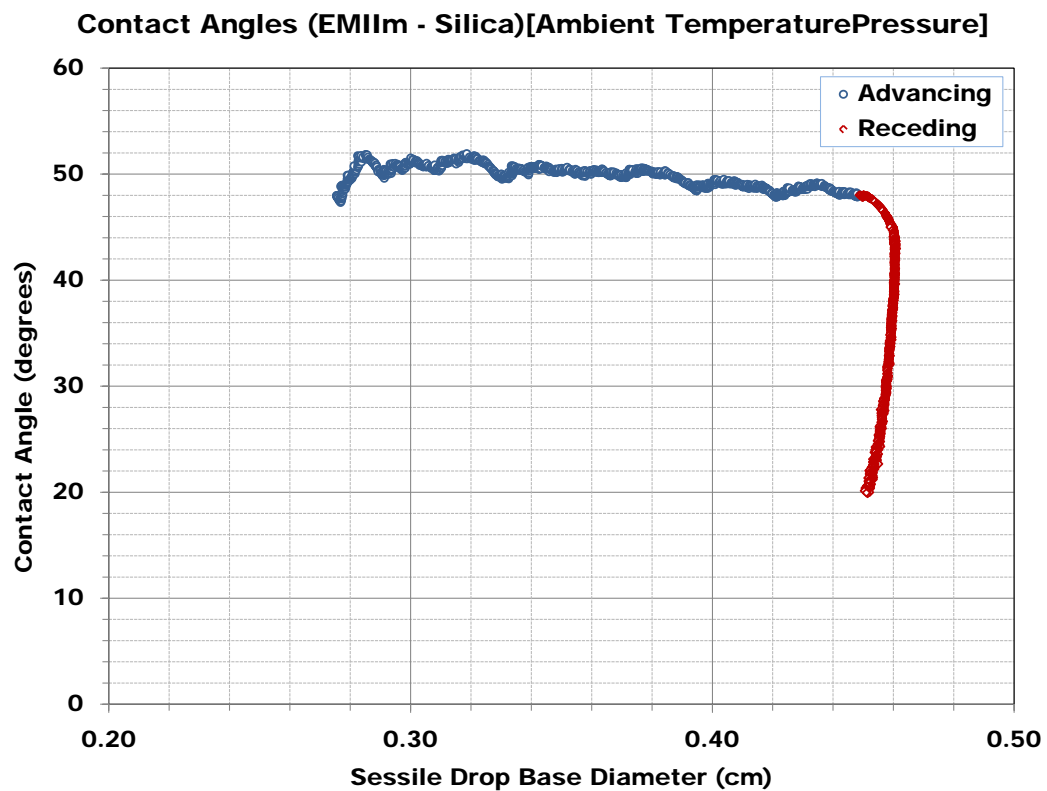

Figure 44: Advancing and receding contact angles taken on fused silica, as a function of droplet base diameter.
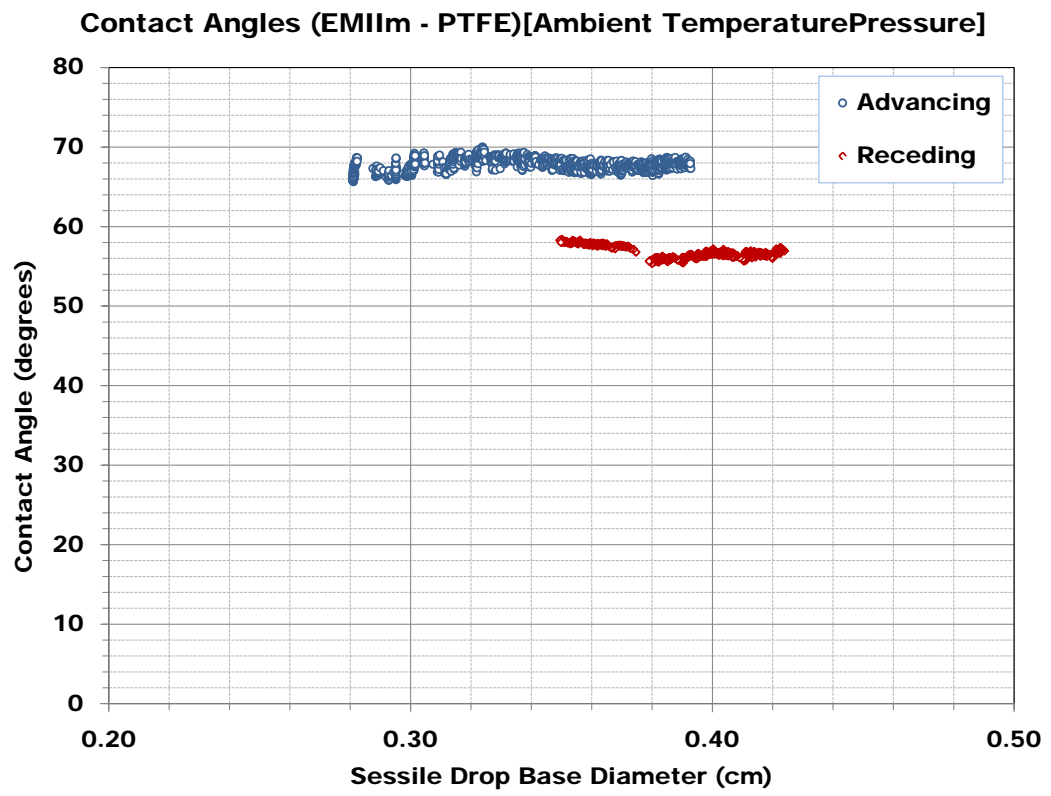
Figure 45: Advancing and receding contact angles taken on Teflon.

Conclusion

The purpose of this research was to record contact angles between EMIIm and different materials useful for electrospray thruster components. This data has been called for in contemporary research and is useful when selecting materials, coatings or surface finish for components that comes in contact with EMIIm. Wetting and surface energy data was recorded for EMIIm wetting eleven different substrates, consisting of nine different materials, under varying operating conditions. Though these measurements exhibited some uncertainties, they represent wetting behavior under realistic conditions and reveal useful properties.

Initial research for this experiment investigated idealized surface science theory, and was used to determine the expected outcome for equilibrium measurements. Data taken noticeably deviated from idealized theory and more research was needed to examine the typical $\pm 5_{\circ}$ deviation and "drift" over time seen in equilibrium contact angles. Further research into surface science theory revealed numerous factors that can cause contact angle formation to deviate from the ideal theory. Chief among these are liquid/solid contamination (chemical reactions) that change their properties and the surface roughness of the solid. Though attempts were made to reduce these factors, they could not be completely removed, explaining the uncertainty and drift in the data. Though not ideal, these measurements are a realistic representation of wetting that would occur on actual electrospray components. Equilibrium and advancing contact angle data as well as the rate of spread observed during equilibrium measurements is summarized in Figure 46.

	Equilibrium Contact Angle (K)	Rate of Spread (n)	Advancing Contact Angle (θ_A)
Less Wetting & Spread	PTFE Teflon (75.9)	PTFE Teflon (0)	PTFE Teflon (68.3)
	Titanium (63.2)	Soda-Lime Glass (-0.0014)	SS316 Fine Grit (58.2)
	SS316 Fine Grit (60.9)	Un-Sintered Tungsten (-0.0015)	SS316 Coarse Grit (55.9)
	Kapton (59.3)	SS316 Mirror Polish (-0.0055)	Soda-Lime Glass (55.2)
	Fused Silica (57.9)	Kapton (-0.0079)	Kapton (52.3)
	SS316 Mirror Polish (57.2)	SS316 Fine Grit (-0.0104)	Titanium (52.3)
	Undoped Silicon (56.4)	Undoped Silicon (-0.0106)	SS316 Mirror Polish (52.1)
	SS316 Coarse Grit (55.1)	Fused Silica (-0.0281)	Fused Silica (51.6)
	Pyrex Slide (45.8)	SS316 Coarse Grit (-0.0285)	Pyrex Slide (49.6)
More Wetting & Spread	Soda-Lime Glass Slide (45.6)	Pyrex Slide (-0.0336)	Undoped Silicon (48.0)
	Un-Sintered Tungsten (39.1)	Titanium (-0.0547)	Un-Sintered Tungsten (43.8)

Figure 46: Individual ranking for each substrate with respect to K, n and θ_A.

PTFE Teflon Behavior

The most striking results among the measurements made were those using the PTFE Teflon substrate. PTFE alone, among all the materials tested, exhibited nearly ideal behavior with practically no spread over time. EMIIm wetting PTFE immediately formed a stable, noticeably high contact angle. A high contact angle indicated that PTFE was the substrate least wetted by EMIIm. This property has many applications with respect to electrosprays as using PTFE components or Selectively coating components with PTFE could be using to control the amount of wetting that occurs. The use of PTFE to reduce the probability of electrospray failure mechanisms is explained further in the following.

Surface Roughness

Techniques to inhibit or promote wetting as desired on a specific substrate were demonstrated during the course of this research. Surface treatment of stainless steel showed that as surface roughness increased for each of the three substrates, the rate at which EMIIm spread over time increased. This result is summarized in Figure 47. This indicates that regions or paths were EMIIm wetting or flow is desired should have a uniform surface roughness to promote wetting/flow. Conversely, any region where wetting is not wanted should be made as smooth as possible to inhibit droplet adhesion and spread. It remains to be investigated as to what degree a surface can be roughened and still increase rate of spread.

Smooth	Surface Roughness	Rate of Spread (n)	Less Spread
	SS316 Mirror Polish (0.634)	SS316 Mirror Polish (-0.0055)	
	SS316 Fine Grit (1.20)	SS316 Fine Grit (-0.0104)	
Rough	SS316 Coarse Grit (2.52)	SS316 Coarse Grit (-0.0285)	More Spread

Figure 47: Relationship between surface roughness and rate of spread n for three different surface treatments of SS316.

Operating Conditions

Temperature and pressure have also been evaluated with respect to wetting characteristics. It was found that pressure variation has no measurable effect on the wetting behavior or surface energy of EMIIm. Though a relationship between wetting properties and pressure is likely, it is on much too small a scale to be evident in this research. However a relationship between temperature and wetting has been demonstrated. Measurements in vacuum

51

between 280 and 327 Kelvin indicated that surface tension is related to temperature, though not in the same way for each material. Some materials agreed with theory and exhibited an inverse relationship with temperature, while most showed a linear trend. Knowing the particular behavior for each material used in electrospray components is significant when evaluating the effect of operating temperature on electrospray performance.

Feed Line Materials

As was showed using the Washburn Equation 17, a lower contact angle, implying more wetting is occurring, results in a higher potential flow rate for a fluid wicking through a capillary. It was determined that, out of the materials tested, Kapton tubing would likely be the ideal material for propellant feed lines. Kapton consistently exhibited the most wetting of the flexible materials that can be manufactured into tubing. Conversely, measurements indicated strongly that PTFE is not the best material for propellant flow lines, especially in a passively fed system. PTFE's high contact angle implies less wicking will occur, therefore PTFE propellant feed lines may result in less mass flow through a passive system. For many externally wetted systems, propellant is stored in a pool and allowed to flow via capillary transport to an external emitter. Flow paths could be established and/or enhanced by applying a surface roughness as previously discussed.

Emitter Materials

Electrospray emitters, whether porous or capillary, externally or internally fed, are required to be easily wetted by the propellant. Contemporary research has shown that emitter made of poorly wetted solid materials can have feed issues. The results of this research indicate that, of the materials tested, Tungsten, Soda-Lime Glass and Fused Silica (though they may be more difficult to fabricate) appear to be the most easily wetted materials. Although emitter tips are required to be easily wetted, we have shown previously that certain areas of the emitter such as the chamfer of an internally wetted emitter may benefit with less wetting. One possibility implied by this research would be to coat the chamfer with PTFE, inhibiting propellant engulfment of the entire tip. Engulfment has been shown to contribute to feed line bubble formation as well as limiting the proximity between the emitter tip and extraction grid, reducing the probability of arcing.

Grid Materials

Electrospray grids are generally required to be conductive and, as we have shown, be poorly wetted by the liquid propellant. For EMIIm it is recommended that the Silicon, a commonly used extraction and acceleration grid material, be used due to it's low propensity for wetting. Wetting could be further decreased by applying coatings of PTFE, which could also

have the added benefit of adding an extra layer of electrical insulation. The benefit would be two-fold as errant droplets would not spread out on the PTFE coating and block more spray apertures, and the extra layer of insulation would serve to reduce the probability of arcing.

Final Thoughts

Electrospray thrusters are an emerging technology option for high ΔV, low thrust propulsion. This research was an effort to help identify compatible materials for an electrospray, firing EMIIm, similar to those installed on the LISA Pathfinder mission. We have shown that wetting can have a significant effect on electrospray operation and have identified both electrospray failure mechanisms and possible benefits and weaknesses associated with different materials. Wetting behavior due to material, surface treatment and temperature must be taken into account during the electrospray design process. It is hoped that this data and consequent analysis will offer insight into materials selection to improve electrospray reliability.

Future Work

Future work of interest includes testing on EMIIM that has been dessicated to a lower water content using a nitrogen titration process. This would yield EMIIm with a water content comparable to contemporary research ($< 10^3 ppm$), possibly leading to more stable/accurate results. Testing other ionic liquid propellants using a similar process would broaden the knowledge base of electrospray propellants and their properties. Testing other ionic liquids might also allow calculation of the critical surface energies of the solid materials already tested, by developing a Zisman plot. It would also be of interest to test a wider array of substrates to broaden the number of materials evaluated for electrospray components. As this paper shows, Teflon is the only substrate that actively resists adhesion with EMIIm. Identifying an electrically conductive material or surface treatment with similar wetting properties would be useful. With more time and effort it would be beneficial to better investigate the relationship between temperature and contact angle, possibly determining why many of the substrates tested did not follow the theory in this respect.

Appendix

A: Surface Roughness Measurements

This appendix presents surface roughness topography measurements taken on several of the substrates tested using an optical laser profilometer. Measurements were taken using a STIL CHR 150 chromatic confocal controller. The CHR 150 was equipped with an OP10000, 10 mm optical "pen" sensor. The sensor was mounted on a 3-axis translation system allowing topographic mapping of each substrate. A 5 mm by 5 mm section was scanned for each of the substrates and two surface roughness machining standards. These surface maps are shown below in Figures 48-52. MountainsMap Topography XT® software was provided by STIL. This software was used to automatically calculate the surface roughness after leveling the data and removing threshold outliers. Surface roughness (R_a) values were calculated over a 3D cross section of substrate according to EUR 15178 EN standard. The software applies a Gaussian filter, then uses Equation 22 to calculate surface roughness, where Z_{xy} is the altitude coordinate at x and y, referenced from the mean altitude.

$$R_a = \frac{1}{nm} \sum_{x=0}^{n-1} \sum_{y=0}^{m-1} |Z_{xy}| \tag{22}$$

Kapton was the smoothest substrate successfully measured with an R_a value of 0.144 μm. The highly reflective or optically transparent substrates such as undoped silicon, fused silicon, Pyrex and glass saturated the optical sensor. These surfaces are assumed to have a surface roughness less than that of Kapton ($R_a < 0.144\mu m$) and are likely much less. Substrates that were successfully measured for surface roughness include the PTFE Teflon, three different surface treatments of stainless steel 316, titanium, tungsten and kapton. R_a values for the two standards tested were %98 and %68 accurate according to their official values of ($R_a = 12.5\mu m$) and ($R_a = 1.6\mu m$) respectively.
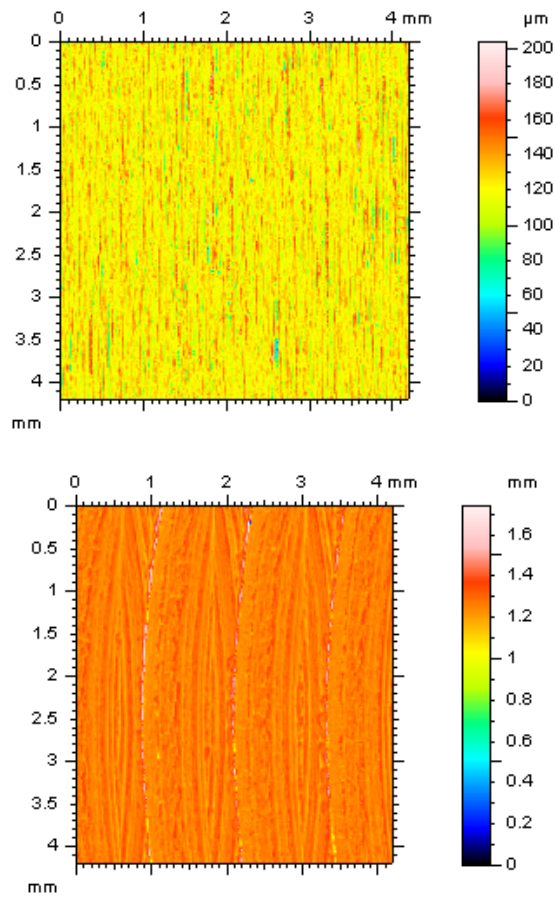
Figure 48: (Top) Surface map of 12.5 μ_m, calculated R_a: 12.2 μm (Bottom) Surface map of 1.6 μ_m, calculated R_a: 2.36 μm
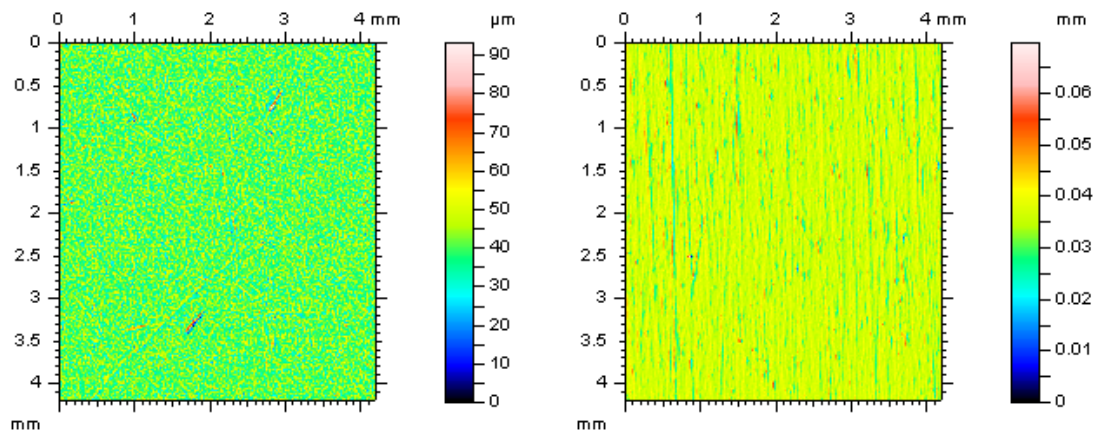

Figure 49: (Left) Surface map of tungsten, calculated R_a: 0.351 μm (Right) Surface map of SS 316 (mirror finish), calculated R_a: 0.634 μm
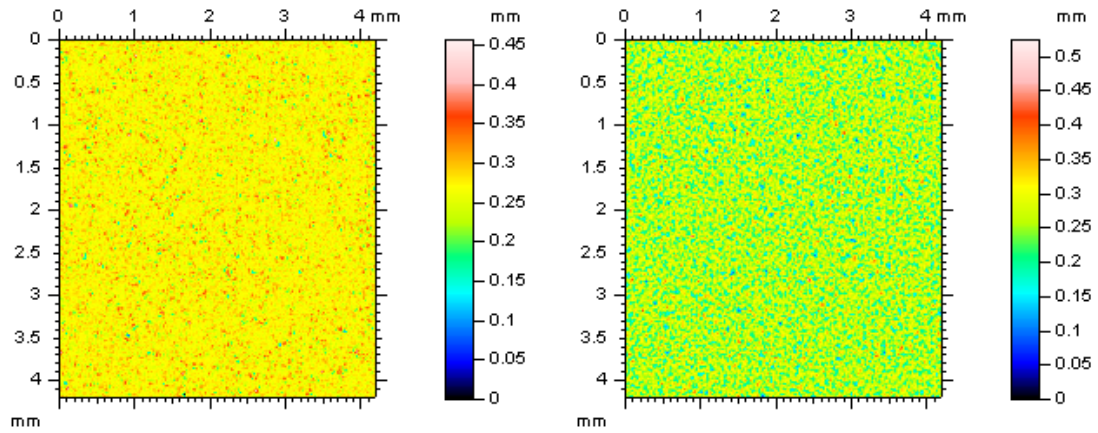
Figure 50: (Left) Surface map of SS 316 (fine grit finish), calculated R_a: 1.20 μm
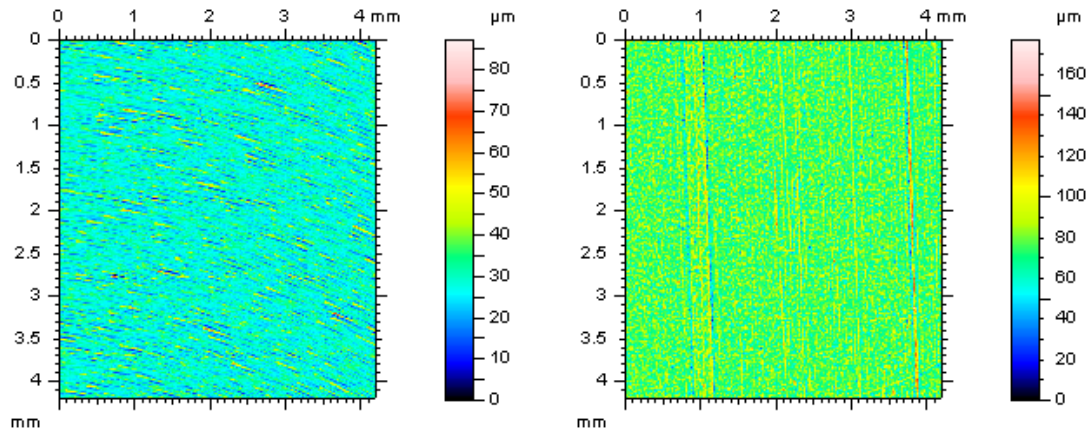(Right) Surface map of SS 316 (coarse grit finish), calculated R_a: 2.52 μm

Figure 51: (Left) Surface map of titanium, calculated R_a: 0.600 μm
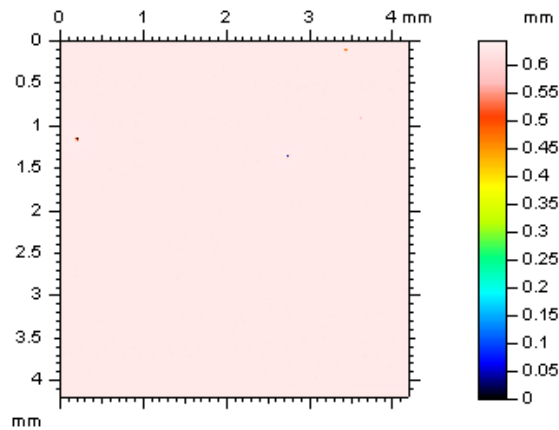(Right) Surface map of PTFE Teflon, calculated R_a: 1.47 μm

Figure 52: Surface map of Kapton, calculated R_a: 0.144 μm

References

[1] Humble, R. W., Henry, G. N., and Larson, W. J., *Space Propulsion Analysis and Design*, The McGraw-Hill Companies, Inc., revised, first ed., 1995.

[2] W.C., E., "Space Vehicle Systems Engineering Handbook," Prepared by: The Aerospace Corporation, National Systems Group for Deputy Director for Systems Engineering, National Reconnaissance Office.

[3] Conroy, D. D. and Ziemer, D. J., "Water Contaminant Mitigation in Ionic Liquid Propellant," Vol. 31, 2009, pp. 1, 2, 8.

[4] Velásquez-Garca, L. F., Akinwande, A. I., and MartnezSánchez, M., "A Planar Array of Micro-Fabricated Electrospray Emitters for Thruster Applications," Vol. 15, 2006, pp. 1273, 1274.

[5] Legge, R. S. and Lozano, P. C., "Electrospray Propulsion Based on Emitters Micro-facbricated in Porous Metals," Vol. 27, 2010, pp. 486, 489, 494.

[6] Urdiales, J. M. L., *Progress in Colloid Propulsion*, Master's thesis, 2004.

[7] Kreitinger, N., *Temperature Effects on Electrospray Performance*, Master's thesis, 2011.

[8] Oh, H., Kim, K., and Kim, S., "Characterization of Deposition Patterns Produced by Twin-Nozzle Electrospray," Vol. 39, 2008, pp. 805, 807.

[9] Ziemer, J. K., Randolph, T. M., and Franklin, G. W., "Colloid Micro-Newton Thrusters for the Space Technology 7 Mission," Vol. 10, 2010, pp. 1, 5.

[10] Kilaru, P., Baker, G. A., and Scovazzo, P., "Density and Surface Tension Measurements of Imidazolium-, Quaternary Phosphonium-, and Ammonium-Based Room-Temperature Ionic Liquids: Data and Correlations," Vol. 52, 2007, p. 2306.

[11] Alexander, M. S., Smith, K. L., Paine, M. D., and Stark, J. P. W., "Voltage-Modulated Flow Rate for Precise Thrust Control in Colloid Electrospray Propulsion," Vol. 23, 2007, p. 1046.

[12] Lozano, P. and Martnez-Snchez, M., "Ionic liquid ion sources: characterization of externally wetted emitters," Vol. 21, 2005, pp. 417,.

[13] Velasquez-Garcia, L. F., Martnez-Snchez, M., and Akinwande, A. I., "Two-Dimensional Micro-fabricated Colloid Thruster Arrays," Vol. 2004, 2004, pp. 3, 5–6.

[14] Velsquez-Garca, L. F., Akinwande, A. I., and Martnez-Snchez, M., "A Micro-Fabricated Linear Array of Electrospray Emitters for Thruster Applications," Vol. 15, 2006, p. 1264.

[15] McNamara, P., "Overview of LISA Pathfinder," Tech. Rep. LISA-LPF-RP-0001, European Space Agency, 2009.

[16] Anderson, John R., P. G. A. M. Z. J., "Testing Fundamental Properties of Ionic Liquids for Colloid Microthruster Applications," 2006.

[17] Pan, Y., Boyd, L. E., Kruplak, J. F., Walter E. Cleland, J., Wilkes, J. S., and Husseya, C. L., "Physical and Transport Properties of Bis(trifluoromethylsulfonyl)imide-Based Room-Temperature Ionic Liquids: Application to the Diffusion of Tris(2,2' -bipyridyl)ruthenium(II)," Vol. 158, 2011, p. F1.

[18] Wandschneider, A., Lehmann, J. K., and Heintz, A., "Surface Tension and Density of Pure Ionic Liquids and Some Binary Mixtures with 1-Propanol and 1-Butanol," Vol. 53, 2008, p. 596.

[19] Jaroslav Klomfar, M. S. and Patek, J., "Surface Tension Measurements for Four 1-Alkyl-3-methylimidazolium-Based Ionic Liquids with Hexafluorophosphate Anion," Vol. 54, 2009, p. 1390.

[20] Carvalho, P. J., Freire, M. G., Marrucho, I. M., Queimada, A. J., and Coutinho, J. A. P., "Surface Tensions for the 1-Alkyl-3-methylimidazolium Bis(trifluoromethylsulfonyl)imide Ionic Liquids," Vol. 53, 2008.

[21] Sigma Aldrich; 3050 Spruce Street, Sain Louis, M. ., "Material Safety Data Sheet, Chemical Name: 1-Ethyl-3-methylimidazolium bis(trifluoromethylsulfonyl)imide, Product#: 11291, CAS#: 174899-82-2," .

[22] Angstroms, F. T., *Application Notes: What are Contact Angles?*, 1997.

[23] Stark, J. P. W., Stevens, B., Alexander, M., and Kent, B., "Fabrication and Operation of Microfabricated Emitters as Components for a Colloid Thruster," Vol. 42, 2005, pp. 628–639.

[24] R.E. Johnson, J. and Dettre, R., *Surface and Colloid Science*, Wiley-Interscience, New York, vol. 2 ed., 1969.

[25] Weston, F. and Zemanski, M. W., *University Physics*, Addison Wesley Inc., 2nd ed., 1955.

[26] Berg, J. C., *Wettability*, Macel Dekker, Inc. New York, surfactant science series, volume 49 ed., 1993.

[27] de Gennes, P.-G., Brochard-Wyart, F., and Quere, D., *Capillary and Wetting Phenomena - Drops, Bubbles, Pearls, Waves*, Springer, 2002.

[28] McMurry, J. and Fay, R. C., *Chemistry*, Prentice Hall, New Jersey, second edition ed., 1998.

[29] Adamson, A. W. and Gast, A. P., *Physical Chemistry of Surfaces*, John Wiley & Sons, Inc., New York, sixth edition ed., 1997.

[30] Kwok D.Y., A. N., "Contact Angle Measurement and Contact Angle Interpretation," 1999.

[31] Schrader, M. E. and Loeb, G. I., *Moder Approaches to Wettability, Theory and Applications*, Plenum Press, New York, 1992.

[32] Wang X., Chen Z., S. Z., "Dynamic Behavior of Polymer Surface and the Time Dependance of Contact Angle," 2005.

[33] Lelah, M. and Marmur, A., "Spreading kinetics of drops on glass," Vol. 82, 1981.

[34] Good, R. J. and Koo, M. N., "The Effect of Drop Size on Contact Angle," Vol. 71, 1979.

[35] Allen, J. S., "An analytical solution for determination of small contact angles from sessile drops of arbitrary size," Vol. 261, 2003.